A direct GABAergic output from the basal ganglia to frontal cortex

HHS Public Access

Author manuscript

Nature. Author manuscript; available in PMC 2015 November 07.

Published in final edited form as:

Nature. 2015 May 7; 521(7550): 85–89. doi:10.1038/nature14179.

A direct GABAergic output from the basal ganglia to frontal cortex

Arpiar Saunders, **Ian A. Oldenburg**, **Vladimir K. Berezovskii**, **Caroline A. Johnson**, **Nathan D. Kingery**, **Hunter L. Elliott**, **Tiao Xie**, **Charles R. Gerfen**, and **Bernardo L. Sabatini***

Department of Neurobiology, Howard Hughes Medical Institute, Harvard Medical School, 220 Longwood Ave, Boston, MA 02115

Abstract

The basal ganglia (BG) are phylogenetically conserved subcortical nuclei necessary for coordinated motor action and reward learning[1]. Current models postulate that the BG modulate cerebral cortex indirectly via an inhibitory output to thalamus, bidirectionally controlled by the BG via direct (dSPNs) and indirect (iSPNs) pathway striatal projection neurons[2–4]. The BG thalamic output sculpts cortical activity by interacting with signals from sensory and motor systems[5]. Here we describe a direct projection from the globus pallidus externus (GP), a central nucleus of the BG, to frontal regions of the cerebral cortex (FC). Two cell types make up the GP-FC projection, distinguished by their electrophysiological properties, cortical projections and expression of choline acetyltransferase (ChAT), a synthetic enzyme for the neurotransmitter acetylcholine (ACh). Despite these differences, ChAT+ cells, which have been historically identified as an extension of the nucleus basalis (NB), as well as ChAT− cells, release the inhibitory neurotransmitter GABA (γ-aminobutyric acid) and are inhibited by iSPNs and dSPNs of dorsal striatum. Thus GP-FC cells comprise a direct GABAergic/cholinergic projection under the control of striatum that activates frontal cortex *in vivo*. Furthermore, iSPN inhibition of GP-FC cells is sensitive to dopamine 2 receptor signaling, revealing a pathway by which drugs that target dopamine receptors for the treatment of neuropsychiatric disorders can act in the BG to modulate frontal cortices.

---

iSPNs are the major dopamine 2 receptor (D2r) expressing cells in the brain and project from dorsal striatum to the GP, suggesting that the therapeutic effects of drugs that target D2rs to treat schizophrenia[6], bipolar disorder[7] and obsessive compulsive disorder[8] may involve GP circuits. GP neurons are generally described as GABAergic, spontaneously

---

*Correspondence and request for materials should be addressed to B.L.S (bsabatini@hms.harvard.edu).

AUTHORS CONTRIBUTIONS

A.S., I.A.O and B.L.S designed the experiments. A.S. performed the anatomical and acute slice experiments, analyzed the data and assisted all other parts of the study. I.A.O performed the *in vivo* recordings and analyzed data. C.A.J assisted with immunohistochemistry experiments and mouse genotyping. V.K.B. performed rhesus macaque anatomical experiments. C.R.G sliced and imaged mouse brains for three-dimensional reconstructions. N.D.K performed the sectioning, staining and imaging for array tomography. H.L.E and T.X. assisted in the image analysis for axon detection in whole-brain reconstructions and array tomography analysis, respectively. A.S. and B.L.S wrote the manuscript with contributions from the other authors.

The authors declare no competing financial interests.

active, and projecting to the thalamus and all nuclei of the BG[9]. Thus the GP is thought to coordinate subcortical activity through inhibition. Nevertheless, there are ChAT$^+$ neurons in and around the GP that project to cortex[10,11] and appear to be innervated by SPNs from dorsal striatum[12,13], despite the rarity of iSPN synapses at the ultrastructural level[14]. In macaques, GP neurons with NB-like firing properties respond to reward[15], a computation attributed to the BG[16]. Furthermore, humans with GP lesions exhibit reduced metabolism in frontal cortices and psychiatric symptoms reminiscent of patients with frontotemporal lobe damage, consistent with loss of substantial extrinsic input[17]. Therefore we examined if the GP contains a projection system to FC that is functionally integrated into BG circuitry.

Retrograde labeling with fluorescent microspheres (retrobeads) in *Drd2*-EGFP mice identified ipsilateral FC-projecting neurons within the GP and clustered on the GP/NB and GP/striatum borders (Fig. 1a; EDFig. 1a–c). Nearly all GP-FC projecting neurons cells express the GABA vesicular transporter (*Vgat*) and synthetic enzyme GAD65 (*Gad2*), while a subset (72%) also express ChAT (EDFig. 1d,e). These results indicate that GP-FC projection neurons may be GABAergic but can be subdivided based on cholinergic marker expression (hereafter ChAT+ and ChAT− cells). ChAT$^+$ cells of the NB also express GABAergic markers[18], suggesting that much of the basal forebrain cholinergic system may corelease GABA (EDFig. 1f,g). ChAT− GP-FC cells do not express parvalbumin (PV) (EDFig. 1h–j); thus they are distinct from GP neurons that project to posterior BG nuclei[19] and other non-cholinergic cortical projecting cells in the basal forebrain[20]. Analysis in a rhesus macaque confirmed that similar classes of neurons are conserved in primates: retrograde labeling followed by ChAT immunostaining identified ChAT$^-$ and ChAT$^+$ cortically-projecting neurons in the GP (EDFig. 2a–e). In both macaque and mouse, ChAT$^+$ cells were distributed around the GP and GP/NB border, areas that in mouse are exposed to iSPN axons (EDFig. 2f,g).

The projection patterns of mouse ChAT− and ChAT+ GP-FC cells were determined by selectively expressing fluorophores in each cell class[21] and analyzing 3-dimensional brain reconstructions (2 mice, EDFig. 3; Sup. Video 1). ChAT+ and ChAT− GP cells target anterior cortices, yet arborize in different but overlapping cortical layers and subcortical nuclei (Fig. 1b–d; EDFig. 4). In most cortical regions, ChAT+ axons arborize in layers 1–6, most densely in layers 1–3, whereas ChAT− axons arborize densely in layers 5 and 6 and are absent from layer 1. In ectorhinal cortex, ChAT− axons extend into layer 1 (EDFig. 3k).

ChAT+ and ChAT− GP-FC cells are electrophysiologically distinct (Fig. 1e–g; EDFig. 5a–f): Retrobead$^+$ ChAT− cells exhibit hyperpolarization activated cation currents (I_h) and, compared to ChAT+ cells, have smaller somata (1,740±391 vs. 5,139±547 μm^3), narrower action potentials, higher maximum firing rates (~200 vs. 30 Hz) and less spike accommodation. ChAT− cells were spontaneously active at all ages studied, whereas ChAT + cells become spontaneously active around sexual maturity (EDFig. 5g) and, once active, have lower firing rates (4.4±0.39 vs. 13.3±1.6 Hz). Thus ChAT expression subdivides these putative GABAergic GP-FC neurons into physiologically distinct cell types that may differentially affect cortical and sub-cortical activity during development and in adulthood.

The influence of this projection on FC was assayed *in vivo* using extracellular recordings in awake, head-fixed mice while optogenetically manipulating GP (Fig. 2 and EDFig. 6). Mice were habituated to restraint and periodically pressed a lever for water reward. Periods without lever presses were analyzed to avoid confounds of motor behavior. Pulsed optogenetic activation (473 nm, 5ms pulses 10 Hz for 3s) of channelrhodopsin (ChR2)-transduced *Vgat*$^{+}$ neurons of GP but not of mCherry-transduced controls entrained firing in FC, as shown by the population activity during the stimulation period and immediately following individual stimuli (ChR2^{+}: n=90 units, 5 mice; mCherry^{+}: n=99 units, 3 mice) (Fig. 2a; EDFig. 6a,b). For each unit the light modulation of activity index (I_{light}) was calculated: I_{light}=0 represents no change in firing, whereas values of +1 or −1 indicate that all firing occurred during light stimulation or non-stimulation periods, respectively. Optogenetic stimulation decreased firing rates ~20% overall ($<I_{light}>$= −0.11±0.02, P<0.0001 Kruskal-Wallis test, Fig. 2a); however, individual units showed increases (~ 4%, n=4 of 90) or decreases (~42%, n=38 of 90, P<0.05, Student's T-test) in firing rate. No significant light-induced changes were observed above chance in controls (n=0 and 2 of 99 units with significantly increased and decreased activity, 3 mice)(EDFig. 6c).

To establish if ongoing activity in GP basally sculpts FC firing, we suppressed GP using the light-driven proton pump archaerhodopsin (ArchT). Constant illumination of ArchT^{+} GP (594 nm, 3 seconds) increased (~26%, n=25 of 96) or decreased (~20%, n=19 of 96) firing of individual FC units (2 mice, P<0.05 Student's T-test, Fig. 2b). These bidirectional changes resulted in no significant change in population firing rate ($<I_{light}>$= 0.02±0.01, P>0.05 Kruskal-Wallis test). Units in mCherry controls (2 mice) were not modulated at a rate greater than chance (n=1 and 2 of 63 units with significant increased or decreased activity, respectively)(EDFig. 6d). In response to ArchT-mediated inhibition or ChR2-mediated excitation of GP, some FC units altered activity within <50 ms of light onset (EDFig. 6e). These gain- and-loss-of-function experiments indicate that activity in GP rapidly, potently and bidirectionally modulates neurons in frontal cortex *in vivo*. Furthermore, local stimulation of ChR2-expresssing GP axons in FC using an optical fiber/electrode combination (optrode) revealed that activity of GP-FC neurons is sufficient to modulate FC. Pulsed illumination of ChR2^{+} axons did not persistently change FC activity, but transiently increased firing rates within 5–10 ms of light onset (n=111 units, 5 mice), an effect not seen in control mCherry^{+} axons (n=92 units, 2 mice) (Fig. 2c; EDFig. 6f,g).

ChAT+ GP-FC axons project heavily to cortex but sparsely within the BG and thalamus (EDFig. 4) such that activation of these cells in GP should minimally engage canonical BG outputs. Pulsed excitation in GP increased firing rates in the FC (n=120 units, 4 mice) by 11% ($<I_{light}>$=0.04±0.01 P<0.0001 Kruskal-Wallis test, Fig. 2d), bidirectionally modulating activity of a subset of individual units (increases: ~13%, n=15 units; decreases: ~2%, n=2). Illumination of ChAT+ axons in FC using an optrode confirmed that these effects were due to activation of GP-FC projection neurons: firing rates transiently increased 5–10 ms after light onset (n=74 units, 3 mice) without persistent changes during the 3s period of pulsed stimulation (EDFig. 6g,h). Lastly, ArchT mediated suppression of ChAT+ GP neurons with constant yellow light did not significant effect firing rates above chance (~1% increased,

n=1 of 120, 4 mice; ~3% decreased, n=3 of 120)(EDFig. 6i), possibly due to low basal firing rate of these cells.

To determine the synaptic mechanisms by which ChAT+ and ChAT− GP-FC cells modulate cortex, we examined the neurotransmitters released by each cell type (Fig. 3; EDFig. 7a,b). Whole-cell voltage-clamp recordings in acute brain slices targeted neurons with somata within ~150 μm of $ChR2^+$ axons (EDFig. 7c). Pharmacology and manipulation of holding potential identified ChR2-evoked synaptic currents due to opening of ionotropic GABA, glutamate, and ACh receptors. In a subset of neurons in FC slices (n=5 of 94 neurons; 5 mice), optogenetic activation of ChAT− axons evoked inhibitory post-synaptic currents (IPSCs) whose properties were consistent with direct GABA release from ChR2-expressing axons and monosynaptic activation of $GABA_A$ receptors (Fig. 3a,b). Similar analysis in subcortical slices of ChR2-expressing ChAT+ axons that ramify around the GP/NB border (ED Fig. 7d–f) revealed excitatory post-synaptic currents (EPSCs) in a small number of cells (n=2 of 85 cells, 6 mice) which were unaffected by application of glutamate receptor antagonists but abolished by nicotinic ACh receptor (nAChR) antagonists (EDFig. 7g–l). In addition, larger and more prevalent IPSCs were detected (n=7 of 85) that were insensitive to antagonists of nAChR and glutamate receptors but were abolished by antagonists of $GABA_A$ receptors (Fig. 3a,b), consistent with direct release of GABA from ChAT+ GP axons and monosynaptic activation of $GABA_A$ receptors. We conclude that both ChAT+ and ChAT− GP-FC cells release GABA, consistent with the expression of markers for GABA synthesis and handling, and that ChAT+ cells additionally release ACh.

Recordings in acute brain slices from mice expressing GFP in cortical GABAergic interneurons identified the FC neurons monosynaptically targeted by each GP-FC cell class (EDFig. 8a–d). Activation of ChAT− axons evoked IPSCs in interneurons in layers 2/3, 5, and 6, as well as pyramidal neurons in layers 5 and 2/3. Activation of ChAT+ axons evoked IPSCs in a small number of interneurons in layers 1, 2/3 and 6 and EPSCs in interneurons in layers 1 and 6. These results suggest ChAT− GP-FC cells inhibit interneurons and pyramidal neurons across cortical layers, whereas ChAT+ GP-FC cells can activate and inhibit cortical interneurons via release of ACh and GABA.

Target-specific neurotransmitter release suggests a separation of GABA and ACh release sites within individual ChAT+ axons in cortex. To examine this possibility, we labeled ChAT+ GP-FC presynaptic terminals (PSTs) with synaptophysin-GFP and determined the proximity of a variety of pre and post-synaptic proteins in ultra-thin brain slices by fluorescence immunohistochemistry (“array tomography”) and custom image analysis routines (Fig. 3c–g; EDFig. 8e–k). Reconstructed portions of FC (8 stacks, 2 mice) contained GFP^+ volumes that resembled “pearls on a string”. Detected GFP^+ “pearls” had volumes consistent with PSTs[22] and co-localized with Synapsin1, Bassoon and GAD1/2, supporting their identity as PSTs capable of synthesizing GABA. GFP^+ PSTs co-localized with Gephyrin but not PSD-95, indicating that they appose inhibitory but not excitatory post-synaptic densities (Fig. 3e). The majority of GFP^+ PSTs immunostained for at least one of the GABA/ACh vesicular transporters (n=4274 of 6071), but all combinations were observed: VAChT alone (n=2030), VGAT alone (n=407) and both VGAT and VAChT (n=1837). Within individual PST expressing both vesicular transporters, the VGAT and

VAChT punctae were separable (318±39 nm between centroids), suggesting that individual axonal boutons can corelease GABA and ACh but do so through distinct vesicular pools (Fig. 3f,g).

ChAT+ GP-FC projection neurons have been previously identified as part of the NB. To be included in the BG, GP-FC cells should receive synaptic inputs typical of the GP: glutamatergic input from the subthalamic nucleus (STN) and GABAergic input from SPNs of the dorsal striatum. Indeed, STN axons arborize in the regions containing GP-FC cells and electrical stimulation of the STN-GP axon tract evoked glutamatergic EPSCs in ChAT+ and ChAT− FC-projecting cells (EDFig. 9a–e). Similarly, axons of iSPNs and, surprisingly, dSPNs ramified around ChAT+ GP neurons (Fig. 4a; Sup. Video 2). Optogenetic stimulation of axons of either striatal cell class evoked GABAergic IPSCs in nearly all GP-FC cells (iSPNs; ChAT+:20 of 22, ChAT−:19 of 20 from 11 mice; dSPNs; ChAT+:12 of 12, ChAT−:11 of 11 from 11 mice, Fig. 4b; EDFig. 10a,b). In contrast, $ChAT^+$ cells of the NB or SI do not receive dorsal SPN input (EDFig. 10c–e). Together these results indicate that GP-FC cells are distinct from NB neurons and are functionally integrated into BG circuitry through direct, indirect and hyperdirect (STN-GP)[23] pathways. Although iSPNs and dSPNs both inhibit GP-FC cells, differences in synaptic strength and short-term plasticity (EDFig. 10b,f,g) suggest that dynamic activity in each pathway could differentially inhibit the GP-FC projection.

The presence of a GABAergic output to cortex under control of striatal SPNs could be important for understanding the etiology and treatment of motor and psychiatric diseases[24,25]. For example, schizophrenia is genetically associated with D2rs[26], treated with drugs that block D2rs[6] and often manifests coincident with developmental changes in cortical inhibition[27]. Schizophrenics exhibit imbalances in GABA[28] and ACh[29] systems, as well as molecular and morphological changes in prefrontal interneurons[30]. Since GP-FC cells are present in primates (EDFig. 2), release GABA and ACh onto interneurons (Fig. 3; EDFig. 8a–d), and are inhibited by D2r-expressing iSPNs (Fig. 4), we examined whether D2r signaling affects iSPN synapses onto GP-FC cells. Indeed, the D2r agonist quinpirole reduced the amplitude of iSPN mediated IPSCs in GP-FC neurons in acute brain slices (Fig. 4c). This reduction was reversed by the antipsychotic sulpiride and was not seen in dSPN mediated IPSCs, confirming that striatal dopamine could disinhibit the GP-FC projection via anti-psychotic sensitive D2r signaling (EDFig. 10h).

The existence of GP-FC cells suggests a major revision to BG models[2,24]. Striatal direct and indirect pathways were proposed to exert opposite effects on cortical activity through bidirectional control of ascending thalamic drive. The GP-FC projections bypass thalamus, allowing dSPNs and iSPNs to modulate cortex in concert. Furthermore, the hyperdirect cortical projection through the STN excites GP-FC neurons directly, forming a two-synapse loop for recurrent cortical modulation. The effects of GP-FC neurons on cortex are complex, mediated by GABA and ACh acting on diverse postsynaptic targets. The context of GP-FC activity during behavior, the specific identities of cortical targets, and the mechanisms and consequences of GABA/ACh co-release will be the subjects of further investigation.

METHODS

Mice

Bacterial artificial chromosome (BAC) transgenic mice expressing EGFP under control of the dopamine 2 receptor locus (*Drd2*-EGFP) were used to define the anatomical border of the globus pallidus externus (GP) and ventral pallidum (VP) through the expression of EGFP in striatal iSPNs (GENSAT, founder line S118). Cre recombinase was targeted to specific cell types of the basal ganglia using knock-in or BAC transgenic mice to drive Cre expression under gene-specific regulatory elements. Cre knock-in mice for *choline acetyltransferase* (*ChAT*)[31] and *Slc32a1* (vesicular GABA transporter or *Vgat*)[32] were generously provided by Brad Lowell (Beth Israel Deaconess Medical Center) and are available from the Jackson Labs (*ChAT* $^{i\text{-}Cre}$, stock #006410; *Vgat* $^{i\text{-}Cre}$, stock #016962). *Gad2* $^{i\text{-}Cre}$ were purchased from Jackson Labs (stock #010802)[33]. All knock-in mice link Cre expression to the gene of interest using an internal ribosome entry site. Targeting Cre expression in dSPNs was achieved with BAC transgenic mice expressing Cre under control of the dopamine receptor 1 (*Drd1a*) or in iSPNs with Cre under control of the adenosine 2A receptor (*Adora2a*) or dopamine receptor 2 (*Drd2*) regulatory elements and obtained from GENSAT (*Drd1a*-Cre, founder EY262, stock #017264-UCD; *Adora2a*-Cre, founder KG139, stock # 031168-UCD; *Drd2*-Cre, founder ER43, stock #017268-UCD)[34,35]. The ChAT-GFP BAC transgenic line used to identify ChAT^{+} neurons was purchased from Jackson Labs (#007902)[36]. To visualize the full processes of Cre expressing cells, Cre mice were bred to Cre-activated TdTomato reporter allele[37] (Ai14; Jackson Labs, stock # 007914; referred to as Rosa26$^{lsl\text{-}tdTomato}$). To visualize the somata of Cre expressing cells, the Cre-activated ZsGreen reporter allele was used[37] (Ai6; Jackson Labs, stock # 007906; referred to Rosa26$^{lsl\text{-}zsGreen}$). To target channelrhodopsin-2 (ChR2) to all Cre expressing cells, Cre driver mice were bred to a Cre-activated ChR2(H134R)-EYFP transgene[38](Ai32; Jackson Labs, stock #012569; referred to as Rosa26$^{lsl\text{-}ChR2\text{-}EYFP}$). In experiments designed to identify cortical cells neighboring ChR2^{+} ChAT+ or ChAT− GP-FC axons as pyramids or interneurons, *ChAT* $^{i\text{-}Cre}$ mice also carried a *Gad1*^{GFP} knock-in allele[39] to highlight a subset of cortical interneurons synthesizing GABA. Unless otherwise noted, we do not distinguish between mice heterozygous (eg $^{Cre/+}$) or homozygous ($^{Cre/Cre}$) for knock-in alleles. Wild type mice refer to C57BL/6 obtained from Charles River. Transgenic mice were of a mixed genetic background. All experimental manipulations were performed in accordance with protocols approved by the Harvard Standing Committee on Animal Care following guidelines described in the US National Institutes of Health *Guide for the Care and Use of Laboratory Animals*.

Virus Preparation

Cre-On or Cre-Off conditional expression was achieved using recombinant adeno-associated virus (rAAV) carrying transgenic cassettes whose transcription was activated or inactivated by Cre[40]. Cre-On conditional expression of channelrhodopsin-2 (ChR2-mCherry, H134R variant), EGFP, mCherry, or Synaptophysin-mCherry was achieved by using a double-floxed inverted open reading frame (DIO). Cre-Off conditional expression of ChR2-mCherry was achieved by starting the open reading frame in the non-inverted orientation with respect to the promoter (DO). To achieve simultaneous Cre-On EGFP and Cre-Off

tdTomato labeling, DIO-EGFP was mixed 1:1 with FAS-tdTomato, an alternative Cre-Off rAAV backbone that achieves Cre-Off expression through excision of the open reading frame using alternative loxp sites[10]. DIO, DO, and FAS rAAVs all use the EF1α promoter and were packaged in serotype 8 by a commercial vector core facility, except for DIO-ArchT-tdTomato which uses a CAG promoter and was packaged as serotype 5 (University of North Carolina). All rAAVs were stored in undiluted aliquots at a concentration $>10^{12}$ genomic copies per ml at −80°C until intracranial injection.

Stereotaxic intracranial injections

Male and female mice (postnatal day 20–120) were anesthetized with isoflurane and placed in a small animal stereotaxic frame (David Kopf Instruments). Under aseptic conditions, the skull was exposed and a small hole was drilled. For rAAVs injections, 200–350 nl total volume was delivered bilaterally into the ventral GP/dorsal NB or 500 nl into dorsal striatum through a pulled glass pipette at a rate of 200 nl·min^{-1} using a Microinject system (World Precision Instruments). GP injection coordinates were 0.7 mm posterior from Bregma, 2.0 mm lateral and 3.8 mm below the pia. Dorsal striatum injection coordinates were 0.9 mm anterior from Bregma, 2.2 mm lateral and 2.5 mm below the pia. After surgical procedures, mice received flunixin for analgesia and were returned to their home cage for >21 days to allow for maximal gene expression. To identify GP neurons that project to frontal cortex, 200 nl of fluorescent retrobeads (Red-1X or Green, Lumafluor) were injected into frontal (anterior to striatum) cortical areas including secondary motor (M2), primary motor (M1), primary somatosensory (S1) and dorsal and ventral agranular insular (AID and AIV) cortices. Frontal cortex injection coordinates were 1.9 mm anterior from Bregma, 1.8 mm lateral and 2 mm below the pia. Following surgery, mice received flunixin and were returned to their home cage for 3–9 days before experimentation. Stereotaxic coordinates were adjusted slightly by age.

Fixed Tissue Preparation and Imaging

Mice were deeply anesthetized with isoflurane and transcardially perfused with 4% paraformaldehyde (PFA) in 0.1 M sodium phosphate buffer (1x PBS). Brains were post-fixed for 1–3 days, washed in 1x PBS and sectioned (40 μm) coronally, sagittally or horizontally using a Vibratome (Leica). Slices were then immunostained (see **Immunohistochemistry**) or mounted on slides (Super Frost). After drying, slices were coverslipped with ProLong antifade mounting media containing DAPI (Molecular Probes) and imaged with an Olympus VS110 slide scanning microscope using the 10x objective. Fluorescent proteins introduced through rAAVs or transgenic alleles were never immunoenhanced, except in 3D brain reconstructions (see **3D brain reconstruction and analysis**). Confocal images (1–2 μm optical sections) were acquired with an Olympus FV1000 laser scanning confocal microscope (Harvard Neurobiology Imaging Facility) through a 63x objective.

Immunohistochemistry

Immunohistochemistry conditions were the same for both mouse and macaque sections. For ChAT immunohistochemistry, slices were incubated in a 1x PBS blocking solution

containing 5% normal horse serum and 0.3% Triton X-100 for 1 hour at room temperature. Slices were then incubated overnight at 4°C in the same solution containing anti-choline acetyltransferase antibody (1:100, Millipore AB144P). The next morning, sections were washed three times for five minutes in 1x PBS then incubated for 1 hour at room temperature in the blocking solution containing donkey anti-goat Alexa 647 or Alexa 488 (1:500, Molecular Probes). For macaque sections, streptavidin conjugated to Alexa 350 or Alexa 488 (1:1000, Molecular Probes) was also included in the secondary reaction to visualize biotinylated dextran amine (BDA) signal. The same protocol was used for NeuN (1:100, Millipore MAB377) and Parvalbumin (1:1000, Millipore MAB1572) immunostaining with anti-mouse Alexa 647 secondary antibodies (1:500, Molecular Probes). Immunostained mouse sections were mounted and imaged as described above. Immunostained macaque sections were mounted as described below.

Retrograde tracing in a Rhesus macaque

A 10 year-old male rhesus macaque was prepared for surgery under aseptic conditions. Anesthesia was initiated with ketamine (15 mg/kg) and valium (1 mg/kg) and the macaque was given an intravenous catheter and intubated. Isoflurane (1–2% in oxygen) was used to maintain anesthesia. Bilateral circular craniotomies were made over the frontal cortex, exposing the principal and arcuate gyri. Tracer injections were targeted to cortical areas that receive projections from the “Ch4id” and “Ch4iv” cell groups[41]. Specifically, tracers were injected along the principal and arcuate gyri (corresponding to the area between Mesulam et al. cases 23, 26 and 6) as well as the ventral orbital frontal cortex (Mesulam case 19) using a micromanipulator to guide a 10 μl Hamilton syringe. In the right hemisphere, Red 1X retrobeads (Lumafluor) were injected at 16 dorsal locations and 4 ventral locations. In the left hemisphere, BDA (10% in sterile saline) was injected at 12 dorsal locations and 2 ventral locations. At each site, 0.5 μl of tracer was injected at 2 depths, 1 and 2 mm below the cortical surface. After injection, the skull fragments were replaced and the macaque was allowed to recover on a water heated pad under constant observation. After a 21 day survival period, the macaque was killed with a barbiturate overdose (>50 mg/kg, to effect) and perfused through the heart with normal saline followed by 4% formaldehyde in 1x PBS, pH 7.4. The brain was removed from the skull and post-fixed for 24 hours in the same fixative solution. Following cryoprotection for 3 days in 30% sucrose solution, the hemispheres were separated, blocked and cut in 40 μm coronal sections using a freezing microtome. Throughout the extent of GP, coronal slices from both hemispheres were sampled 1 out of 12 to check for retrograde labeling. To visualize BDA labeling in the left hemisphere, sliced were rinsed in 1x PBS and immunostained (see **Immunohistochemistry**). Slices from the retrobead-injected right hemisphere were unenhanced. Slices were mounted on gelatin-covered slides using an acetone-xylenes drying procedure then coverslipped with DPX-medium. Sampled sections from the right hemisphere showed non-specific fluorescent microsphere labeling throughout subcortical areas and thus were not considered further. Sampled sections from left hemisphere contained cells with retrograde labeling in the GP/NB area consistent with Ch4iv and Ch4id groups. Flanking sections to those showing retrograde labeling were then double immunostained for ChAT and BDA (see **Immunohistochemistry**) and imaged as above. All experimental manipulations were performed in accordance with protocols approved by the Harvard Standing Committee on

Animal Care following guidelines described in the US National Institutes of Health *Guide for the Care and Use of Laboratory Animals*.

Slice preparation

Acute brain slices were obtained from mice using standard techniques. Mice were anesthetized by isoflurane inhalation and perfused through the heart with ice-cold artificial cerebrospinal fluid (ACSF) containing (in mM) 125 NaCl, 2.5 KCl, 25 $NaHCO_3$, 2 $CaCl_2$, 1 $MgCl_2$, 1.25 NaH_2PO_4 and 11 glucose (~308 $mOsm \cdot kg^{-1}$). Cerebral hemispheres were removed, placed in ice-cold choline-based cutting solution (consisting of (in mM): 110 choline chloride, 25 $NaHCO_3$, 2.5 KCl, 7 $MgCl_2$, 0.5 $CaCl_2$, 1.25 NaH_2PO_4, 25 glucose, 11.6 ascorbic acid, and 3.1 pyruvic acid), blocked and transferred into a slicing chamber containing ice-cold choline-based cutting solution. Sagittal slices (350 μm thick) were cut with a Leica VT1000s vibratome and transferred to a holding chamber containing ACSF at 34°C for 30 minutes and then subsequently incubated at room temperature. Both cutting solution and ACSF were constantly bubbled with 95% O_2/5% CO_2. In a subset of experiments, acute brain slices were cut in ice-cold ACSF.

Acute slice electrophysiology and two-photon imaging

Individual slices were transferred to a recording chamber mounted on a custom built two-photon laser scanning microscope (Olympus BX51WI) equipped for whole-cell patch-clamp recordings and optogenetic stimulation. Slices were continuously superfused (3.5–4.5 $ml \cdot min^{-1}$) with ACSF warmed to 32–34°C through a feedback-controlled heater (TC-324B; Warner Instruments). Cells were visualized through a water-immersion 60x objective using differential interference contrast (DIC) illumination. Epifluorescence illumination was used to identify those cells labeled by fluorescent microspheres and/or expressing fluorescent genetic markers. Patch pipettes (2–4 MΩ) pulled from borosilicate glass (G150F-3, Warner Instruments) were filled either with a Cs^+-based low Cl^- internal solution containing (in mM) 135 $CsMeSO_3$, 10 HEPES, 1 EGTA, 3.3 QX-314 (Cl^- salt), 4 Mg-ATP, 0.3 Na-GTP, 8 Na_2-Phosphocreatine (pH 7.3 adjusted with CsOH; 295 $mOsm \cdot kg^{-1}$) for voltage-clamp recordings, or with a K^+-based low Cl^- internal solution composed of (in mM) 135 $KMeSO_3$, 3 KCl, 10 HEPES, 1 EGTA, 0.1 $CaCl_2$, 4 Mg-ATP, 0.3 Na-GTP, 8 Na_2-Phosphocreatine (pH 7.3 adjusted with KOH; 295 $mOsm \cdot kg^{-1}$) for current-clamp recordings. Alexa Fluor 594 (20 μM) was added to both internals. Series resistance (<25 MΩ) was measured with a 5 mV hyperpolarizing pulse in voltage-clamp and left uncompensated. Membrane potentials were corrected for a ~7 mV liquid junction potential. After the recording was complete, cellular morphology was captured in a volume stack using 740 nm two-photon laser light (Coherent). All recorded GP-FC neurons were labeled with microspheres following injection in frontal cortex. In experiments where ChAT expression was not marked fluorescently, ChAT+ or ChAT− GP-FC neurons were distinguished based on soma size and spontaneous firing rate in cell attached mode. Cortical neurons were classified as pyramids or interneurons based on dendritic morphology and *Gad1*^{GFP} expression. For analyses of intrinsic properties shown in Fig. 1f and EDFig. 5a–f, mice were age post-natal day (P) 18–22. For whole-cell spontaneous firing rates shown in Fig. 1g, all ages assayed (P13-56) were included. For all analyses of intrinsic properties, NBQX (10 μM), CPP (10 μM) and SR95331 (50 μM) were included in the bath. For

pharmacological analyses of synaptic transmission in Fig. 3a,b mice were P66-127. For optogenetic activation experiments of ChAT− cells, NBQX (10 μM) and CPP (10 μM) were included in the bath. For ChAT+ cells, the bath solution was drug-free. IPSCs evoked from ChAT− cells (V_{hold}=0 mV) were blocked by the voltage-gated sodium channel blocker tetrodotoxin (TTX, 1 μm), demonstrating action potential-dependent ChR2-mediated transmitter release. IPSCs could be rescued in the continued presence of TTX by enhancing ChR2-mediated depolarization of terminals with application of the voltage-gated K^+ channel blocker 4-aminopyridine (4AP, 500 μm) and were subsequently abolished in the presence of the $GABA_A$ receptor antagonist SR95531 (50 μM), indicating direct (monosynaptic) release of GABA by ChAT− cells. For the ChAT+ cell type, evoked EPSCs (V_{hold}=−70 mV) were unaffected by application of CPP and NBQX, but abolished by nicotinic receptor antagonist cocktail of MEC (10 μm), MLA (0.1 μm) and DhβE (10 μm), indicative of ACh release and activation of ionotropic nicotinic receptors. IPSCs evoked from ChAT+ activation were blocked by SR95531, but not by CPP, NBQX, MEC, MLA or DHβE, indicating $GABA_A$ receptor activation independent of glutamatergic and nicotinic signaling. ChAT+ IPSCs were blocked by TTX and rescued by 4AP, confirming direct release of GABA by ChAT+ cells. For the screen of cortical synaptic connectivity reported in EDFig. 8b, NBQX and CPP were included in the bath for both ChAT+ and ChAT− GP-FC cell experiments. In a subset these experiments, TTX and 4AP were also included. See EDFig. 8c,d for comparison. For FC layer 1 experiments involving optogenetic activation of all *ChAT* $^{i\text{-}Cre}$ expressing neurons reported in EDFig. 7k,l, mice were age P27-91 and NBQX and CPP were included in the bath. For optogenetic experiments involving iSPNs or dSPNs reported in Fig. 4b,c and EDFig. 10f–h, mice were age P30-37. NBQX, CPP, scopolamine (10 μM), CGP55845 (5 μM) & AM251 (10 μM) were included in the bath and quinpirole (8 μM) and sulpiride (10 μM) were used for flow-ins. For experiments involving optogenetic activation of striatum reported in EDFig. 10e, mice were age P43-45 and NBQX and CPP were included in the bath. For experiments involving electrical stimulation of the STN-GP axons reported in EDFig. 9d,e, mice were age P38-42 and SR95331 was included in the bath.

Acute slice data acquisition and analysis

Membrane currents and potentials were recorded using an Axoclamp 700B amplifier (Molecular Devices) filtered at 3 kHz and digitized at 10 kHz using National Instruments acquisition boards and a custom version of ScanImage written in MATLAB (Mathworks). Electrophysiology and imaging data were analyzed offline using Igor Pro (Wavemetrics), ImageJ (NIH), MATLAB (Mathworks) and GraphPad Prism (GraphPad Software). In figures, voltage-clamp traces represent the average waveform of 3–6 acquisitions; current-clamp traces are individual acquisitions. Passive membrane properties were calculated from current deflections in voltage-clamp (V_{hold} = −70 mV). Cells were considered spontaneously active with maintained action potential firing (>20s) within 2 minutes of whole-cell break in. Average V_{rest} was calculated for non-spontaneously active cells 1–3 minutes after break in. Peak amplitudes were calculated by averaging over a 1 ms window around the peak. In EDFig. 9d,e, AMPAR and NMDAR currents were isolated from the stimulation artifact by subtracting the NBQX resistant component (V_{hold} = −70 mV) followed by the CPP/NBQX resistant component (V_{hold} = +40 mV) following a 3 minute wash-in period from current averages consisting of 10–15 consecutive acquisitions (20 s

inter-stimulus interval). For pharmacological analyses in Fig. 4c current averages were calculated from 15 consecutive acquisitions (20 s inter-stimulus interval) before and after a 3 minute wash-in period and then normalized to averages corresponding to the same time with no drug flow in. For pharmacological analyses in Figs. 3a,b, 3–7 consecutive acquisitions (20 s inter-stimulus interval) were averaged following a 3 minute wash-in period for NBQX and CPP or a 4 minute wash-in period for MEC, MLA, and DHβE. For TTX and 4AP conditions, current averages were composed of the acquisitions following full block or first-recovery of ChR2 evoked currents, respectively. Current responses reported in EDFig. 8b were considered monosynaptic if present in TTX/4AP or <3.1ms onset latency. Data (reported in text and figures as mean ± s.e.m.) were compared statistically using the following Mann-Whitney test or Fisher's Exact test. P values smaller than 0.05 were considered statistically significant.

Optogenetic and electrical stimulation in acute slices

To activate ChR2 in acute slices, 473 nm laser light (Optoengine) was focused onto the back aperture of the 60x water immersion objective to produce collimated whole-field illumination. Square pulses of laser light were delivered every 20 seconds and power was quantified for each stimulation by measuring light diverted to a focal plane calibrated photodiode through a low-pass dichroic filter. For ChR2 introduced with rAAVs, light (2 ms;1.3–4.4 $mW{\cdot}mm^{-2}$) was used across conditions except in some cases following bath application of TTX and 4AP where increasing the power or duration of light stimulation was necessary to recover currents (for example, changing the duration from 2 to 4 ms). For ChR2 activation of dSPN or iSPN inputs onto GP-FC cells (*Drd1a*-Cre;Rosa26$^{lsl\text{-}ChR2\text{-}EYFP/+}$ or *Adora-Cre*;Rosa26$^{lsl\text{-}ChR2\text{-}EYFP/+}$ mice), a consistent light stimulation (1 ms; 1.3 $mW{\cdot}mm^{-2}$) was delivered directly over the recorded cell and the resulting currents were used to compare synaptic strength across cells. For pharmacological analysis reported in Fig. 4c and EDFig. 10h and paired-pulse comparisons reported in EDFig. 10f,g, the objective was moved 0.16 – 1.4 mm into dorsal striatum (median = 0.4 mm) and stimulation strength and duration (0.5–1 ms; 0.06–4.4 $mW{\cdot}mm^{-2}$) were adjusted to produce 1st peak currents between 26 – 547 pA (median = 226 pA). Stronger light powers (2–7 ms;4.4 $mW{\cdot}mm^{-2}$) were used activate ChR2 in *ChAT* $^{i\text{-}Cre}$ cells (*ChAT* $^{i\text{-}Cre}$;Rosa26$^{lsl\text{-}ChR2\text{-}EYFP/+}$ mice) in cortex (EDFig. 7k,l). For electrical activation of the STN axonal projection into the GP, a bipolar tungsten electrode (TST33A10KT; World Precision Instruments) was placed at the anterior border of the STN and 0.1–0.5 ms square pulse of current was applied and power adjusted to maintain evoked currents while minimizing the stimulus artifact.

Reagents

Drugs (all from Tocris) were applied via bath perfusion: SR95531 (10 μM), tetrodotoxin (TTX; 1 μM), 4-aminopyridine (4AP; 500 μmu;M), scopolamine (10 μM), (2*S*)-3-[[(1*S*)-1-(3,4-Dichlorophenyl)ethyl]amino-2-hydroxypropyl](phenylmethyl)phosphinic acid (CGP 55845; 5 μM), *N*-(Piperidin-1-yl)-5-(4-iodophenyl)-1-(2,4-dichlorophenyl)-4-methyl-1*H*-pyrazole-3-carboxamide (AM-251; 10 μM), 2,3-dihydroxy-6-nitro-7-sulfamoyl-benzo(*f*)quinoxaline (NBQX; 10 μM), *R*,*S*-3-(2-carboxypiperazin-4-yl)propyl-1-phosphonic acid (CPP; 10 μM), *N*,2,3,3-Tetramethylbicyclo[2.2.1]heptan-2-amine, (MEC; 10 uM), [1α, 4(*S*),6β,14α,16β]-20-Ethyl-1,6,14,16-tetramethoxy-4-[[[2-(3-methyl-2,5-dioxo-1-

pyrrolidinyl)benzoyl]oxy]methyl]aconitane-7,8-diol (MLA; 0.1 uM), (2*S*,13b*S*)-2-Methoxy-2,3,5,6,8,9,10,13-octahydro-1*H*,12*H*-benzo[*i*]pyrano[3,4-*g*]indolizin-12-one (DHβE; 10 uM), (*S*)-(−)-5-Aminosulfonyl-*N*-[(1-ethyl-2-pyrrolidinyl)methyl]-2-methoxybenzamide ((−)sulpiride; 10 μM) and (4a*R*-trans)-4,4a,5,6,7,8,8a,9-Octahydro-5-propyl-1*H*-pyrazolo[3,4-*g*]quinolone ((−)quinpirole; 8 uM). CPP and NBQX were combined to make a cocktail of antagonists to target ionotropic glutamate receptors, while MEC, MLA and DHβE were combined to make a cocktail to antagonize nicotinic receptors.

Biocytin labeling of STN axonal projections

Acute parasagittal slices (350 μm thick, 10° off-sagittal) were prepared from wild type mice (post natal day 34) as described above. This cutting orientation preserves the reciprocal connections between the subthalamic nucleus (STN) and the GP[42]. In circulating warm ACSF (32–34°C), patch pipets filled with biocytin (0.2%, Molecular Probes) containing internal solution containing (in mM) 135 mM $KMeSO_4$, 5 mM KCl, 5 mM HEPES, 4 mM Mg-ATP, 0.3 mM Na_2-Phosphocreatine (pH 7.4 adjusted using KOH; 295 mOsm·kg^{-1}) were targeted to the STN under DIC illumination. A picospritzer (Picospritzer III; Parker Instrumentation) was used to puff the solution into the center of STN for 1 hour (400 ms pulse at 1 Hz, 5–10 PSI). The slice was allowed to recover for 0.5 hour before being transferred to 4% PFA in 1x PBS overnight. The following morning, slices were rinsed in 1x PBS before avidin-biotinylated HRP complex (ABC) processing (Vectastain)[43]. Slices were then wet-mounted onto glass slides, coverslipped, and imaged under bright-field illumination using the 10x objective of an Olympus VS110 slide scanner microscope.

In vivo electrophysiology

At least 1 week after the initial injections, male mice were surgically implanted with a permanent titanium headpost. In this surgery the coordinates for GP, FC, and M1 were marked on the surface of the skull based on stereotaxic coordinates. The headpost was secured and the animal's skull was covered with C&B metabond (Parkell Inc). Animals were subsequently housed alone and allowed to recover for 1 week before habituation to restraint. Mice were water restricted (to a target of 85% of their free feeding weight) and habituated to restraint in a custom-made lever-press training rig. This rig allows the animal to press a lever in response to an auditory cue. Animals were trained for increasing durations for at least 3 days until they were able to tolerate head restraint for 90 min without struggling. In this time animals achieved an intermediate level of performance on the task, where they knew the association between lever press and reward, but were not proficient at recognizing and responding to tones. One day before the first recording day animals were anesthetized with isoflurane and received a craniotomy over the region of interest. In this surgery, if necessary, a chronic fiber (62.5μm core multimode fiber (ecablemart.com) attached to a ceramic LC ferrule (Pfp Inc) was implanted at the same coordinates as the GP viral injection, but at depth 2.8mm. All Chronic fibers were prescreened to have >80% transmission at 473nm light. A ceramic ferrule connecter linked the chronic fiber to a standard LC cable. Light shuttering and output control was through an acousto optic modulator (AA systems) and had >1000:1 occlusion ratio. Recordings were made using 16 or 32 channel silicone probes with 177 μm^2 recording sites (Neuronexus Technologies) spaced 50 μm apart and lowered to a depth of ~1000μm below the surface of the brain.

Optrode recordings were made with a 16 channel probe of the same configuration fitted with a fiberoptic 100 μm above the top recording site (Neuronexus Technologies, OA series). Stimulation intensity for blue light fiber stimulation was 5 mW from fiber tip (~ 400 $mW{\cdot}mm^{-2}$), optrode stimulation was 10 mW from fiber tip (~ 800 $mW{\cdot}mm^{-2}$) and yellow light fiber stimulation was 3 mW from fiber tip (tip (~ 250 $mW{\cdot}mm^{-2}$). All *in vivo* electrophysiology was acquired using the omniplex system (Plexon Inc) and filtered at 300–8KHz. Spike detection was done by level crossing generally at 50μV and clustering to remove the noise cluster using offline sorter (Plexon Inc). Units that were separable were counted separately, but many units were accepted as multi-unit. All analysis here assumes each unit as a possible multi-unit and is only separated when necessary. Units with firing rate <0.1Hz in the baseline period were excluded for analysis. All analysis was performed using custom scripts in Igor Pro. Data visualization and statistical analysis was done using Igor Pro and GraphPad Prism. *Index of Modulation (I_{Light})* was calculated as the difference in firing rate with the light on, minus the firing rate of the light off divided by the sum of those firing rates, it varies from −1 to 1 where a 0 indicates no change and 1 indicates all activity was detected with the light on. *Latency analysis* was carried out similar to other groups[44], firing rate for each unit was binned in 50ms periods aligned to the onset of optogenetic stimulation. Mean and standard deviation (SD) of the firing rate was determined for a baseline period 1s long ending with the light onset. The first bin after light onset to deviate more than ±2 SD from the baseline mean was reported as the bin of first change. Units where no change was detected within the first 500ms were ignored. By this metric units can have both an increasing and decreasing first bin irrespective of the net change in firing rate. *Z score of ms timescale firing rate changes* was calculated by obtaining a mean and standard deviation of firing in 20 x 5ms bins from a baseline period 3s prior to each 5ms blue pulse. This baseline period had the same number of pulses as the actual stimulation trial (4500–6000 pulses) but was shifted to a period of no illumination. The actual firing rate was z-scored (mean subtracted and divided by the SD) by this baseline mean and SD, to find significant deviations. Z scores from each unit were averaged to create a population value (Fig. 2c, EDFig. 6g). All mCherry control experiments were performed in *ChAT* $^{i\text{-}Cre}$ mice following transduction of rAAV DIO-mCherry in the GP. All ArchT experiments were performed in *Vgat* $^{i\text{-}Cre}$ or *ChAT* $^{i\text{-}Cre}$ mice following transduction of rAAV DIO-ArchT-tdTomato into the GP.

Three-dimensional brain reconstruction and analysis

Following fixation, brains were frozen and sectioned at 50 μm. GFP and tdTomato were immuno-enhanced in free floating sections using mouse-anti GFP (1:1000, abCam ab1218) and rabbit-anti RFP (1:2000, Rockland Antibodies 600-401-379) followed by anti-mouse Alexa 488 (1:200, Jackson Immunoresearch 115-545-062) and anti-rabbit Cy3 (1:2000; Jackson Immunoresearch 111-165-144) secondary antibodies. Sections were mounted on slides and counterstained with Neurotrace Blue (Invitrogen) and imaged on a Zeiss microscope with a Ludl motorized stage controlled with Neurolucida software (Microbrightfield). Imaging was done with a 10x objective and a Hamamatsu Orca Flash 4 camera. Each coronal section containing between 80–200 tiles merged with Neurolucida software. Coronal sections were aligned and Nissl labeling normalized using Neurolucida, Adobe Photoshop and ImageJ software. Aligned sections were rendered in three dimensions

and cortical areas defined using Imaris software (Bitplane). Custom algorithms were written in MATLAB (Mathworks) to detect and quantify axons by cortical area. Briefly, 2D multiscale hessian filtering[45] was followed by non-maximum suppression and then by hysteresis thresholding[46]. Hysteresis thresholds were applied to both the response (largest eigenvalue of hessian) and anisotropy (difference of eigenvalues after normalizing by Gaussian filter response). For anterior-posterior analysis of axon densities (Fig. 1c), raw data was 5 point median filtered and peak normalized. For average fluorescence measurements across layers (Fig. 1d), fluorescence signal from each channel was normalized to peak and baseline subtracted by white matter signal.

Array Tomography

Mice were deeply anesthetized with isoflurane and transcardially perfused with 4% PFA, 2% Sucrose in 0.1 M sodium phosphate buffer (1x PBS). Brains were post-fixed for 1 day, washed in 1x PBS and sectioned into 300 μm sagittal slabs using a Vibratome (Leica). Frontal cortex was then cut out using a razor blade and dehydrated through a series of alcohol dilutions before being infiltrated with LR White acrylic resin (Sigma Aldrich L9774-500G) overnight. Tissue was then placed in a LR White filled gel cap that was polymerized at 50°C overnight. Blocks of tissue were cut on an ultramicrotome (Leica EM UC7) into ribbons of 70 nm thin sections. Sections were then manually lifted onto gelatin coated slides, air dried and then heated on a hot plate (~80°C) for ten minutes. Slides were marked by Pap Pen liquid blocker. Ribbons were treated with 50 mM glycine in 1x TBS for 5 minutes, followed by 5 minutes in blocking buffer (5% BSA, .05% Tween 20 in TBS) before primary antibody staining. Staining was performed in blocking buffer overnight at 4° C. After primary antibody staining, the slides were washed three times with TBS, followed by blocking buffer for five minutes. Secondary antibody staining was performed in blocking buffer for 30 minutes at room temperature. All secondary antibodies were used at a dilution of 1:150. Slides were washed with TBS, then rinsed with ultrapure H_2O for 20 seconds. SlowFade Gold antifade reagent with DAPI (Molecular Probes S36939) was added to each slide before coverslipping. After imaging, the coverslip was removed and the slide was treated with elution buffer (0.2M NaOH, 0.1% SDS in dH_2O) for 20 minutes at room temperature. The slide was washed with TBS three times and rinsed with ultrapure H_2O for 20 seconds. After rinsing, each slide was allowed to air dry, then put on a hot plate for 10 minutes before staining. Subsequent stains followed the same protocol. The dilutions and staining order are as follows:

1. Stain 1: chkαGFP 1:100(GTX13970, GeneTex); musαGephyrin 1:100(612632, Biosciences Pharmingen); rabαGAD 65–67 1:1000(ab11070, Abcam)
2. Stain 2: rabαPSD95 1:100(3450, Cell Signaling Tech.)
3. Stain 3: musαBassoon 1:100 (ab82958, Abcam); rabαSynapsin 1 1:100 (5297S, Cell Signaling Tech.)
4. Stain 4: rabα Parvalbumin 1:100(PV-25, Swant)
5. Stain 5: musαVAChT 1:100(139 103, Synaptic Systems); rabαVGAT 1:100(131 011, Synaptic Systems)

Imaging was performed using a Zeiss Axio Imager Z1 Upright Fluorescence Microscope. A position list was generated at 20x in cortex to identify the ROI on each section. Four images were then acquired with Zeiss Plan-Apochromat 63x/1.4 Oil DIC Objective and stitched into a single final image (Mosaix, Axiovision). Individual stacks were aligned in FIJI using the MultiStackReg plugin, initially using the DAPI channel and then a second alignment to the stack from the first imaging session. Fine alignments were the performed using the Synapsin1 stack and the Register Virtual Stack Slices plugin of FIJI to correct for warping. Background fluorescence was then subtracted from the aligned stacks using a 10 pixel rolling ball filter and contrast was adjusted to 0.1% through the FIJI software. Image analyses were carried out with custom written scripts in MATLAB (Mathworks). GFP^+ volumes and diffraction-limited synaptic markers were computationally detected from image stacks. GFP^+ "pearls", which correspond to putative pre-synaptic terminals (PSTs), were identified as varicosities belonging to a "string" with multi-plane spanning volumes. All synaptic markers were treated as single pixel point-sources within a given z plane. Images were segmented to exclude $DAPI^+$ nuclei and areas containing no tissue. Co-localization analyses of GFP^+ "pearls" and synaptic markers were performed by quantifying the mean voxel densities within GFP^+ "pearls" (0 distance) and from 102–512 nm outside "pearl" volumes. Mean voxel densities for real data were compared to those mean densities (EDFig. 8i) following randomization of diffraction-limited immunopunctae (1000 rounds). Z scores (as in Fig. 3e; EDFig. 8k) were calculated from 0 distance mean densities following 10 rounds of GFP^+ "pearl" randomization:

$$Z\ Score = \frac{(mean_{real} - mean_{random})}{\sqrt{\left(\frac{{\sigma_{real}}^2}{n_{real}} + \frac{{\sigma_{random}}^2}{n_{random}}\right)}}$$

In total, the array tomography dataset consisted of n=8 stacks from n=2 mice, with n=4 stacks in layers 1–3 and n=4 stacks in layer 5. Each stack consisted of 26–31 x 70 nm slices, with a total volume of $7.6 \times 10^5\ \mu m^3$. Note, in the plot in Fig. 3f, which reports the distances between VGAT-VAChT punctae within the same GFP^+ "pearl," excludes n=8 singleton values between 1.2–1.6 μm.

Extended Data

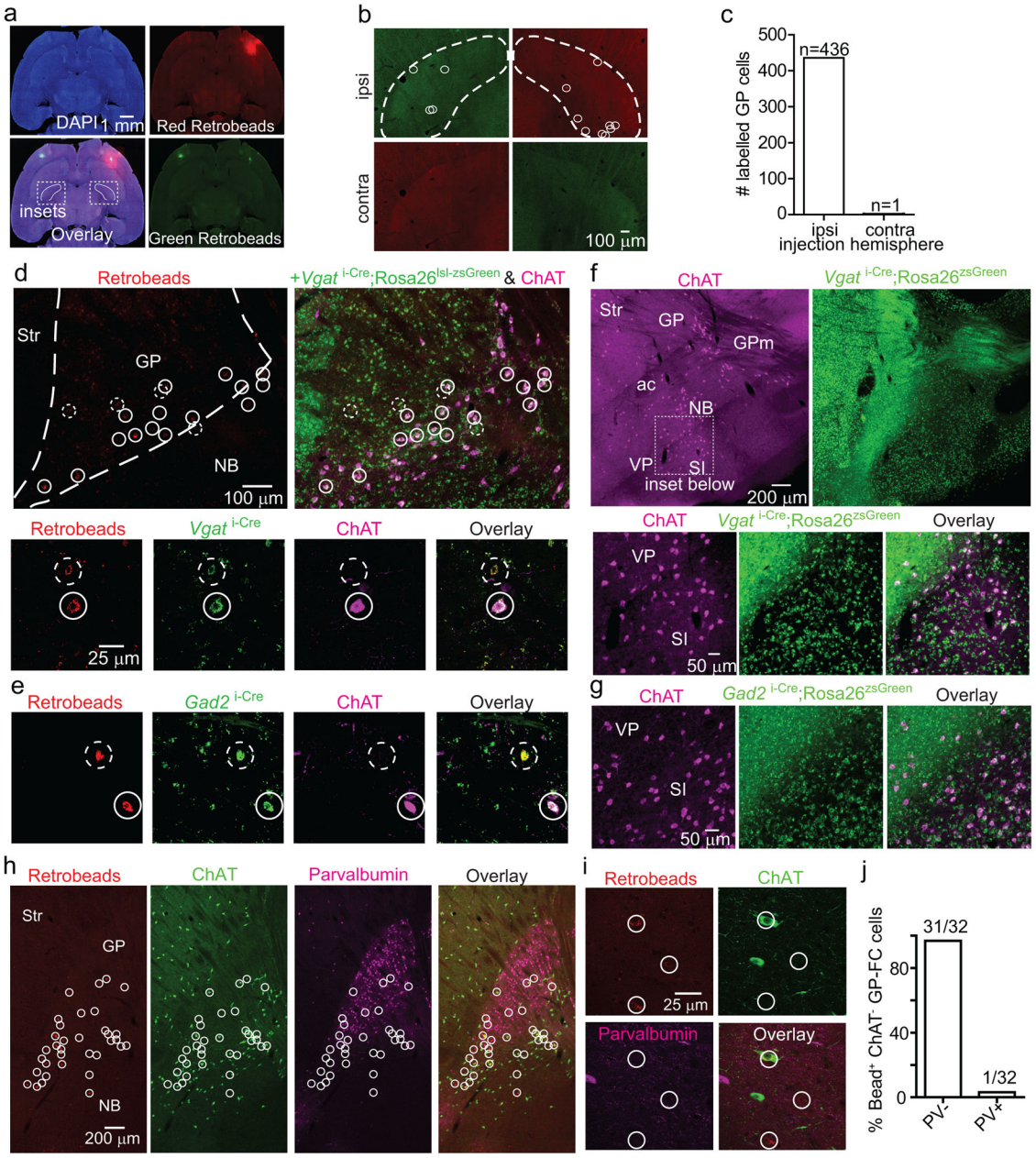

Extended Data Figure 1. Anatomical and molecular properties of GP-FC cells and ChAT$^+$ cells of the substantia innominata (SI) and ventral pallidum (VP)

a–c. GP-FC cells project exclusively to ipsilateral cortex. **a.** Low magnification horizontal section from a wild type mouse injected bilaterally in FC with red (right hemisphere) and green (left hemisphere) retrobeads. DAPI (blue), nuclear stain. Boxed insets show location of GP in **b.** Green signal in the right hemisphere is due to bleed through from the red channel. **b.** High magnification of left and right GP from the same brain as in **a.** Retrobead$^+$ cells from ipsilateral (ipsi) and contralateral (contra) injections are highlighted with white

circles. Dashed lines demarcate the approximate boundaries of the GP. **c.** Summary graph showing nearly all retrobead^{+} cells (n=436 of 437, from 4 mice) resulted from injections in ipsilateral FC. **d–e.** FC retrobead labeling in *Vgat* $^{i\text{-}Cre}$;Rosa26$^{lsl\text{-}zsGreen}$ or *Gad2* $^{i\text{-}Cre}$;Rosa26$^{lsl\text{-}zsGreen}$ mice followed by ChAT immunostaining (magenta) demonstrates that nearly all retrobead^{+} GP cells (red) are *Vgat* $^{i\text{-}Cre\ +}$ or *Gad2* $^{i\text{-}Cre\ +}$ (green) while a subset of retrobead^{+} neurons are also ChAT^{+} (solid circles) and the remainder are ChAT^{-} (dashed circles). Nearly all retrobead^{+} GP cells were *Vgat*$^{+}$ (n=159 of 159 cells, from 3 mice) or *Gad2*$^{+}$ (n=231 of 233 cells, from 2 mice), whereas 72% were ChAT^{+} (n=215 of 300 cells, from 5 mice) and 28% ChAT^{-} (n=85 of 300 cells). **d**. *Top*, low magnification sagittal view of the GP. *Bottom*, a single confocal plane from stacks used to quantify marker co-localization in *Vgat* $^{i\text{-}Cre}$;Rosa26$^{lsl\text{-}zsGreen}$ mice. **e.** A single confocal plane from stacks used to quantify marker co-localization in *Gad2* $^{i\text{-}Cre}$;Rosa26$^{lsl\text{-}zsGreen}$ mice. **f–g.** ChAT^{+} neurons of the substantia innominata (SI) and ventral pallidum (VP) also express *Vgat* and *Gad2*. **f.** *Top*, low magnification ventral view of a sagittal section from a *Vgat*$^{i\text{-}Cre}$; Rosa26$^{lsl\text{-}zsGreen}$ mouse immunostained for ChAT. *Bottom*, high magnification view of the SI and bordering VP. **g.** High magnification view of SI/VP in a *Gad2* $^{i\text{-}Cre}$; Rosa26$^{lsl\text{-}zsGreen}$ mouse immunostained for ChAT. **h–j.** ChAT− GP-FC cells do not express Parvalbumin (PV). **h.** Low magnification view of sagittal section through the GP of a wild type mouse injected with retrobeads (red) in FC and immunostained for ChAT (green) and PV (magenta). White circles highlight retrobead^{+} GP-FC cells. **i.** A single confocal plane showing retrobead^{+} GP-FC cells (circled in white) and immunostaining for ChAT and PV. **j.** Confocal quantification of co-localization between retrobead^{+} ChAT^{-} GP-FC cells and PV (n=32 cells, from 2 mice).

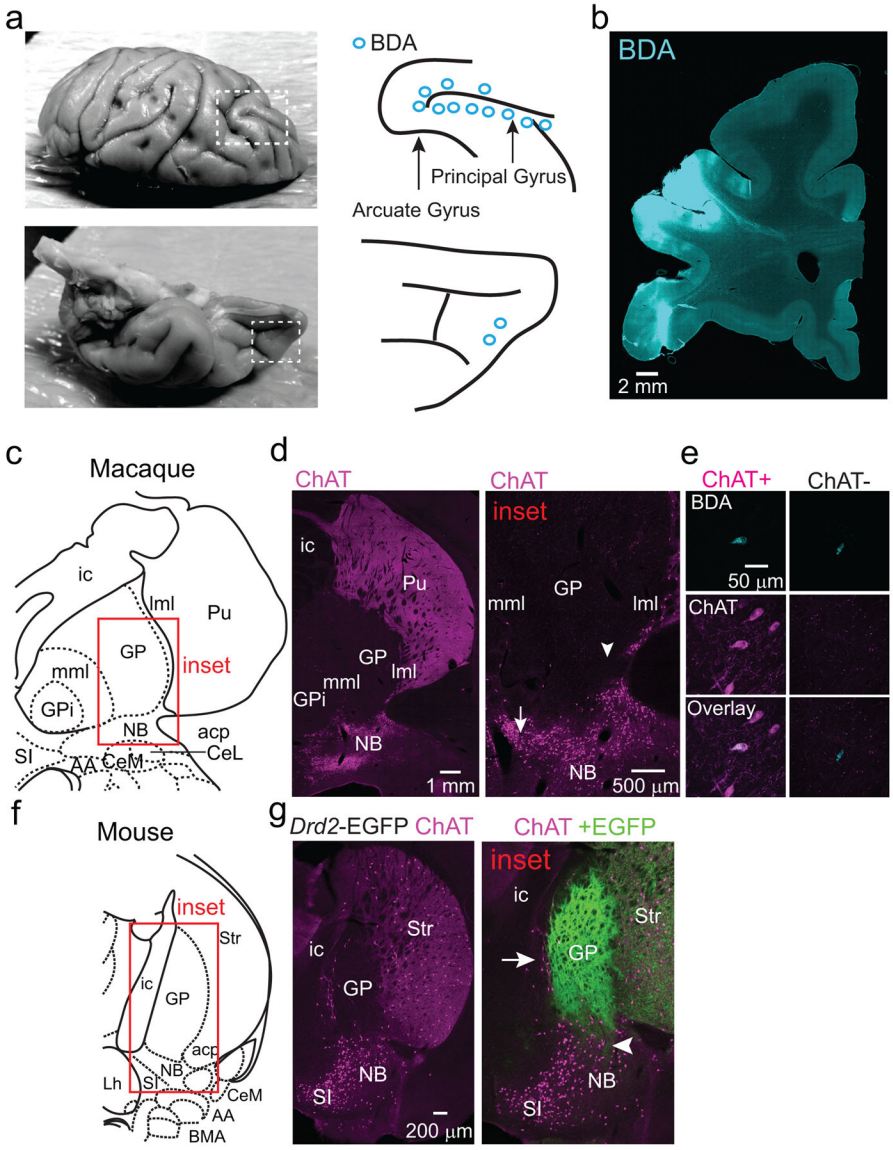

Extended Data Figure 2. ChAT+ and ChAT− GP-FC cells are present in a rhesus macaque

a. In order to label frontal cortical projection neurons from Ch4iv and Ch4id regions of the NB adjacent to the GP of a rhesus macaque[30], the neuronal tracer biotinylated dextran amine (BDA) was injected at multiple sites along the arcuate and principal gyri and in the orbital cortex. *Left*, dorsal (*top*) and ventral (*bottom*) views of a fixed macaque brain. Dashed boxes indicate the injected areas. *Right*, schematic of the injection sites. Blue circles correspond to 2 x 0.5 µl BDA injections at 1 and 2 mm below the pial surface. **b.** Coronal section through the injection area after immunostaining to visualize BDA. **c–e.** Immunostaining for BDA and ChAT identifies retrogradely labeled ChAT+ and ChAT− GP-FC cells. **c.** Coronal section from macaque atlas containing GP and NB. **d.** *Left*, ChAT immunostaining highlights traditional anatomical boundaries of the GP/Putamen and GP/NB. Same plane as in **c**. *Right*, higher magnification view of GP/NB border corresponding to the inset in **c**. $ChAT^{+}$ neurons are distributed around the ventral GP/dorsal NB and along laminae

separating the GP from the Putamen (lateral medullary laminae, lml) and GPi (medial medullary laminae, mml). Arrow and arrowhead indicate approximate locations of $BDA^{+}ChAT^{+}$ (680 μm anterior) and $BDA^{+}ChAT^{-}$ (360 μm anterior) example GP-FC cells shown in **e. e.** Single confocal planes showing example $BDA^{+}ChAT^{+}$ and $BDA^{+}ChAT^{-}$ GP-FC cells. **f,g.** ChAT immunostaining in a *Drd2*-EGFP mouse distinguishes traditional anatomical boundaries of the GP/NB from the territory occupied by iSPN axons. **f.** Coronal section from the mouse atlas. **g.** *Left*, ChAT immunostaining highlights traditional anatomical boundaries of the GP/Striatum and GP/NB. Same plane as in **f**. *Right*, higher magnification view of GP/NB border region corresponding to the inset in **f**. As in macaque, $ChAT^{+}$ cells are distributed along GP borders between striatum and the internal capsule (ic) and at the border of ventral GP/dorsal NB. Overlay of GFP fluorescence demonstrates iSPN axons arborize throughout the GP, abutting $ChAT^{+}$ cells on the GP border regions (arrow), and ventrally in the dorsal NB (arrowhead). AA, anterior amygdaloid area; ac, anterior commissure posterior; CeL, central lateral division of amygdala; CeM, central medial division of amygdala; GP, globus pallidus externus; GPi, globus pallidus internus; Lh, lateral hypothalamus; Pu, putamen; SI, substantia innominata; Str, striatum.

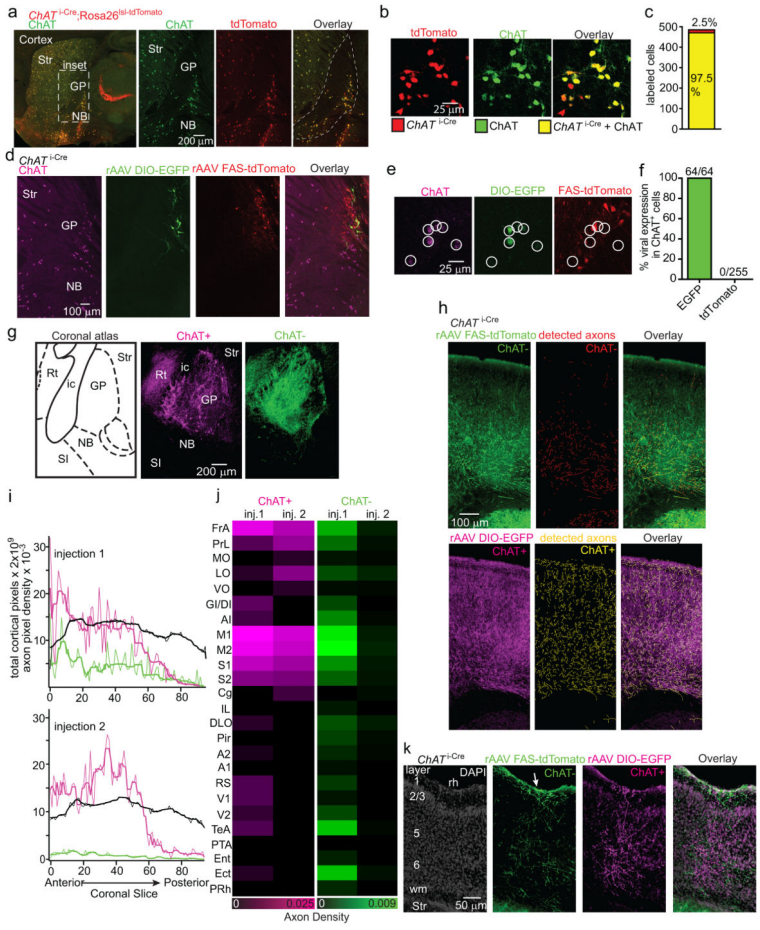

Extended Data Figure 3. Validation of *ChAT* $^{i\text{-}Cre}$ knock-in mouse and rAAV strategy for Cre-On/Off labeling of GP-FC axons in cortex

a–c. The *ChAT* $^{i\text{-}Cre}$ mouse expresses Cre selectively in ChAT^{+} GP/NB neurons with high penetrance. **a.** *Left*, low magnification view of sagittal section through *ChAT* $^{i\text{-}Cre}$;Rosa26$^{lsl\text{-}tdTomato}$ mouse immunostained for ChAT. *Right*, inset showing higher magnification view of the GP and NB. Dashed line approximates the boundaries for quantifying Cre-reporter and ChAT co-localization. **b.** Single confocal plane showing overlap of Cre-reporter expression and ChAT immunostaining of ChAT^{+} cells at the GP/NB border. **c.** Quantification of confocal co-localization between the Cre-reporter^{+} and ChAT^{+} cells (n=471 of 484 tdTomato^{+} ChAT^{+}, n=12 of 484 tdTomato^{+} only, n=1 of 484 ChAT^{+} only, from 3 mice). **d–f.** Transduction of the GP in a *ChAT* $^{i\text{-}Cre}$ mouse with DIO-EGFP (Cre-On) and FAS-tdTomato (Cre-Off) rAAVs effectively targets GFP and tdTomato to ChAT^{+} and ChAT^{-} cells respectively. **d.** Sagittal section through the GP following transduction of the DIO-EGFP (green) and FAS-tdTomato (red) rAAVs and immunostaining for ChAT (magenta). **e.** Single confocal plane showing ChAT^{+} cells (circled in white) co-localized with GFP but not tdTomato. **f.** Quantification of confocal co-localization between ChAT, GFP and tdTomato (n=319 ChAT^{+} cells, from 2 mice). **g.** *Left*, coronal atlas. *Right*, injection site for injection 1 (Fig. 1b–d), showing ChAT+ (Cre-On) expression limited to GP and the immediately adjacent NB. ChAT− (Cre-Off) expression is limited to GP with slight leak in striatum. ChAT+ and ChAT− axons arborize in Rt. SI, substantia innominata; NB, nucleus basalis; ic, internal capsule. **h.** Coronal section of anterior M1 illustrating automated axon detection of ChAT− and ChAT+ axons. **i.** Densities of detected ChAT− (green) and ChAT+ (magenta) axons along with total cortical area (black) in successive 50 μm coronal slices (anterior-posterior) across the cortical mantle (n= 2 mice). Densities and area are shown raw (thin line) and after 5 point median filtering (thick line). Median filtered data are reported in Fig. 1c. j. Average density of ChAT+ and ChAT− GP-FC axons by cortical area. FrA, frontal association; PrL, prelimbic; MO, medial orbital; LO, lateral orbital; VO, ventral orbital; GI/DI, granular/dysgranular; AI, agranular insular; M1, primary motor; M2, secondary motor; S1, primary sensory; S2, secondary sensory; Cg, cingulate; IL, infralimbic; DLO, dorsolateral orbital; Pir, piriform; A2, secondary auditory; A1, primary auditory; RS retrosplenial; V1, primary visual; V2, secondary visual; TeA, temporal association; PTA, parietal; Ent, enthorhinal; Ect, ectorhinal; PRh, perirhinal. **k.** Coronal section illustrating the distribution of GP-FC axons across layers of ectorhinal cortex, a posterior cortical area that receives a large GP-FC projection. ChAT− axons target superficial layers 1 and 2/3 (arrow), in addition to deeper layers 5 and 6, as in anterior cortices including M1. The ChAT+ axons arborize across all cortical layers in both ectorhinal and anterior cortical areas. rh, rhinal fissure; Str, striatum; wm, white matter.

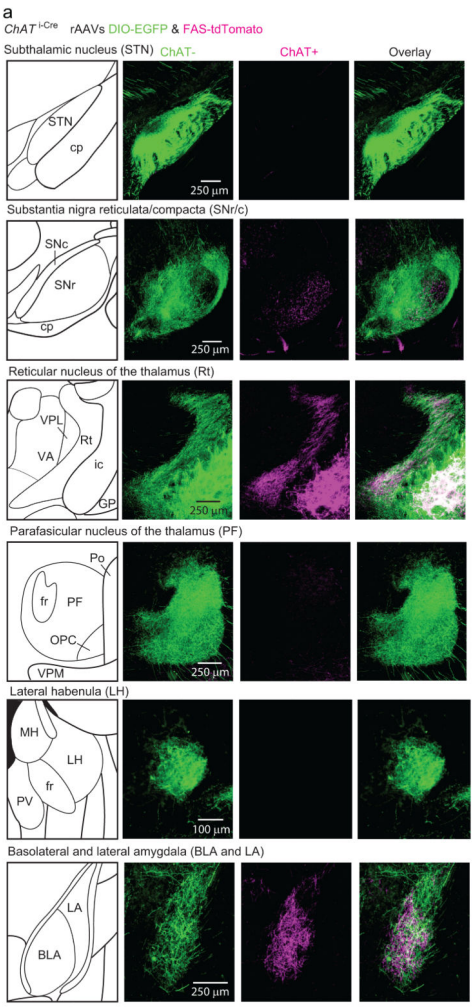

Extended Data Figure 4. ChAT+ and ChAT− GP-FC cells target distinct but overlapping subcortical nuclei

a. Coronal sections from a three dimensional brain reconstructions illustrating subcortical nuclei targeted by ChAT+ and ChAT− axons following transduction of *ChAT* $^{\text{i-Cre}}$ GP/dorsal NB with rAAVs DIO-EGFP (green, Cre-On) and FAS-tdTomato (magenta, Cre-Off) (n=2 mice, examples from injection 1). *Left*, coronal atlas. *Right*, high magnification views of subcortical nuclei.

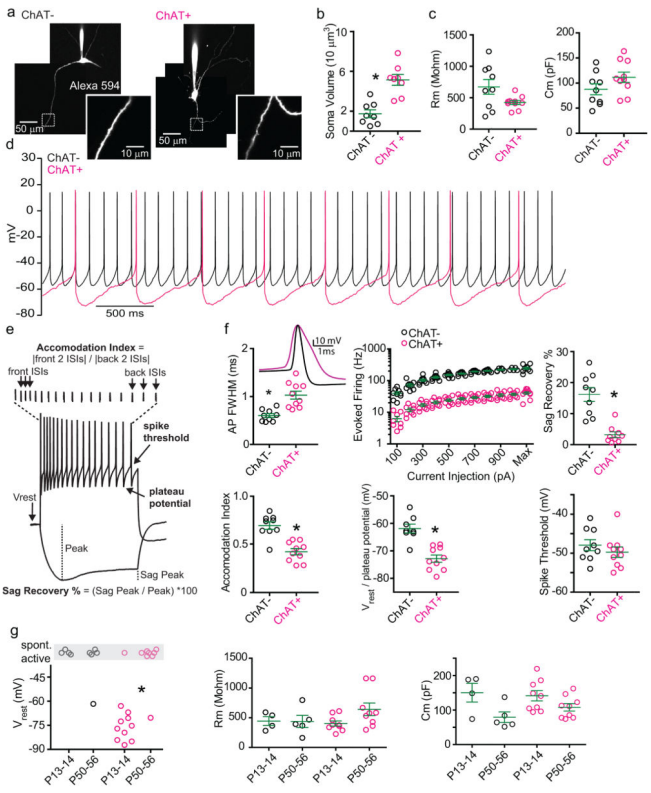

Extended Data Figure 5. GP-FC cells are distinguished by active and passive membrane properties

a. Maximum intensity 2-photon projections of example ChAT− (*left*) and ChAT+ (*right*) GP-FC cells following whole-cell recording. Dashed insets show high magnification projections through dendrites. **b.** ChAT+ cells have larger soma than ChAT− cells. Soma volumes were quantified from 2-photon stacks (from 4 P18-22 mice; n=8 ChAT+ cells, n=8 ChAT− cells). **c.** Passive membrane properties of GP-FC cells (n=9 ChAT−, n=10 ChAT+, from 4 P18-22 mice). **d.** Representative waveforms of spontaneously active ChAT− and ChAT+ GP-FC cells. **e.** Schematic of quantified membrane properties following positive and negative current injections. ISI, interspike interval. **f.** Active membrane properties of GP-FC cells (n=8–9 ChAT−, n=10 ChAT+). Representative action potential waveforms from a spontaneously active ChAT− cell or from minimal current injection in a ChAT+ cell. Evoked firing rates were calculated for 500 ms current injections. **g.** Developmental comparison of GP-FC membrane properties before (P13-14, n=2 mice) and around (P50-56, n=3 mice) sexual maturity. *Left*, ChAT− GP-FC cells are spontaneously active throughout post-natal development (P13-14, n= 4 of 4; P50-56, n=4 of 5), while ChAT+ cells tend to become spontaneously active after sexual maturity (P13-14, n=1 of 11; P50-56, n=7 of 8). GP-FC membrane resistance (*middle*) does not change before and after sexual maturity but membrane capacitance (*right*) is reduced (ChAT−: P13-14, n= 4; P50-56, n=5; ChAT+: P13-14, n= 9; P50-56, n=9). Asterisk, $P<0.05$ (Fisher's Exact test); Bars denote mean±s.e.m.

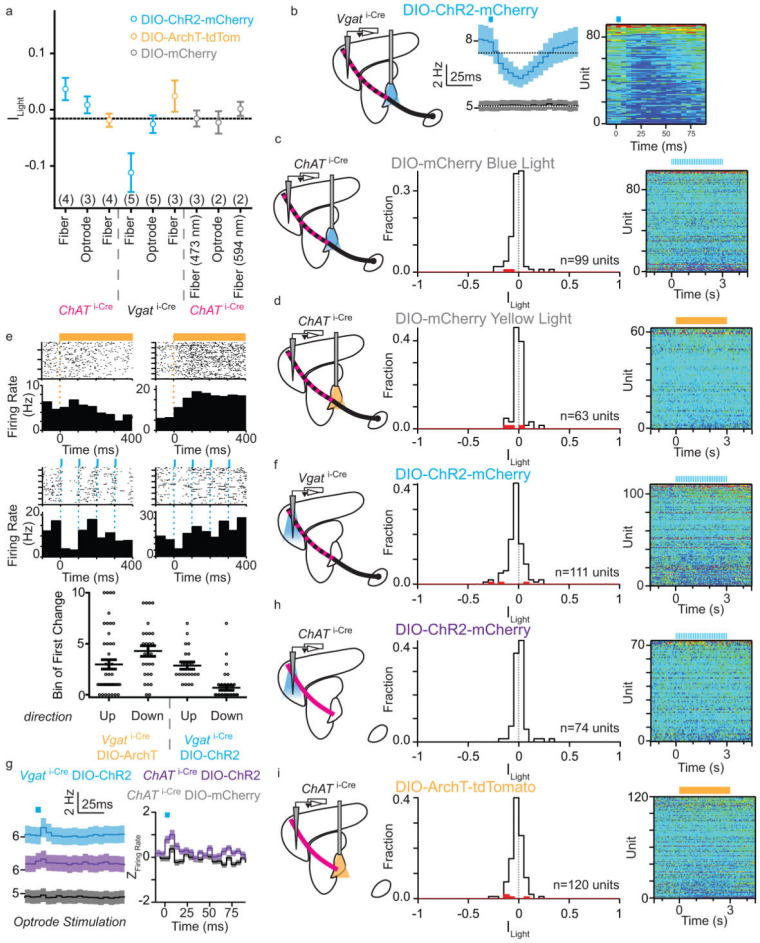

Extended Data Figure 6. Optogenetic manipulations of GP-FC cells coupled with *in vivo* extracellular FC recordings in an awake behaving mouse

a. Summary plot of mean (and 95% CI) indices for light modulation (I_{light}) of FC unit firing rate by experimental condition. Dashed line denotes average of blue light fiber mCherry^{+} control. The number of mice for each condition are shown in parentheses. **b.** Pulsed ChR2 depolarization of *Vgat* $^{i\text{-}Cre}$ GP somata in FC increases firing rates on a millisecond time scale. *Left*, experimental schematic. Extracellular recordings in FC are coupled with fiber-delivered pulses of blue light (5ms pulses of 473 nm, 10 Hz for 3s) in GP. *Middle*, mean firing rate (±sem) of all FC units in response to pulsed blue light in ChR2^{+} (blue) or control (black) mice (ChR2^{+}, n=90 units from 5 mice; mCherry^{+}, n=99 units from 3 mice). Dotted line represents mean pre-stimulation firing rate. *Right*, pseudocolored plot of normalized firing rate for all units. **c.** Fiber-delivered pulsed blue light illumination of mCherry^{+} GP somata in *ChAT* $^{i\text{-}Cre}$ mice shows no light induced changes in the firing rates of FC units above chance (Increased, 0 of 99; Decreased, 2 of 99; from 3 mice). *Right*, pseudocolored plot of normalized firing rate for all units. **d.** Fiber-delivered constant yellow light illumination of mCherry^{+} GP somata in *ChAT* $^{i\text{-}Cre}$ mice shows no light induced changes in the firing rates of FC units above chance (Increased, 1 of 63; Decreased, 2 of 63; from 2 mice;). *Right*, pseudocolored plot of normalized firing rate for all units. **e.** Latencies of light-induced modulation of FC firing following fiber-based illumination of ChR2^{+} (pulsed blue

light) or ArchT^{+}(constant yellow light) GP somata in *Vgat* $^{i\text{-}Cre}$ mice. *Top*, spike raster blots (upper) and firing rate histograms (lower, 50ms bins) from example FC units exhibiting light-induced decreases and increases in firing rates. Onset times for light pulses are shown with colored dash lines. *Bottom*, summary graph plotting light-effect latencies for those FC units with statistically significant modulations. Firing rates are binned every 50 ms, such that "Bin of first change = 0" contains the spikes from 0–50 ms after light onset. First change is determined as the first bin to deviate more than ± 2 SD from the mean baseline firing. Units in which no change is detected within 500 ms are excluded. Individual units may have a first increasing and first decreasing bin if their activity is biphasic. Mean 50 ms bin of first activated by ArchT in *Vgat* $^{i\text{-}Cre}$ mice was 3.0±0.5 n = 47 of 96 units; first suppressed 4.3±0.5 n = 28 of 96 units; first activated by ChR2 2.9±0.3 n = 22 of 90 units, first suppressed by ChR2 0.7±0.2 n = 35 of 90 units. **f.** Optrode-delivered pulsed blue light illumination of ChR2^{+} axons in FC from *Vgat* $^{i\text{-}Cre}$ mice shows no persistent changes in the firing rates of FC units above chance (Increased, 1 of 111; Decreased, 2 of 111 from 5 mice). *Right*, pseudocolored plot of normalized firing rate for all units. **g.** Pulsed blue light illumination of GP-FC axons using an optrode leads to increases in firing rate on the millisecond timescale. *Left*, mean (±sem) firing rates on a millisecond time scale of all units in response to pulsed blue light illumination of GP axons in FC for *Vgat* $^{i\text{-}Cre}$ mice expressing ChR2 (blue) or mCherry (black) or *ChAT* $^{i\text{-}Cre}$ mice expressing ChR2 (purple). *Right*, Z score of inter-pulse interval firing rates (20 x 5ms bins) comparing positive and negative deviations from preceding baseline period without light. **h.** Optrode-delivered pulsed blue light illumination of ChR2^{+} axons in FC from *ChAT* $^{i\text{-}Cre}$ mice shows no persistent changes in the firing rates of FC units above chance (Increased, 0 of 74 from 3 mice; Decreased, 0 of 74). *Right*, pseudocolored plot of normalized firing rate for all units. **i.** Fiber-delivered constant yellow light illumination of ArchT^{+} GP somata in *ChAT* $^{i\text{-}Cre}$ mice shows no light induced changes in the firing rates of FC units above chance (Increased, 1 of 120; Decreased, 3 of 120 from 4 mice). *Right*, pseudocolored plot of normalized firing rate for all units. In plots of I_{light}, red bars indicate units that were statistically significantly modulated by light (T-Test, $P<0.05$). For pseudocolored plot of normalized firing rate, units are normalized to the baseline period, prior to light onset, and ordered by I_{light} (low to high). Blues and purples represent low firing rates whereas yellow and red represent higher firing rates. Red represents modulations three or more times baseline.

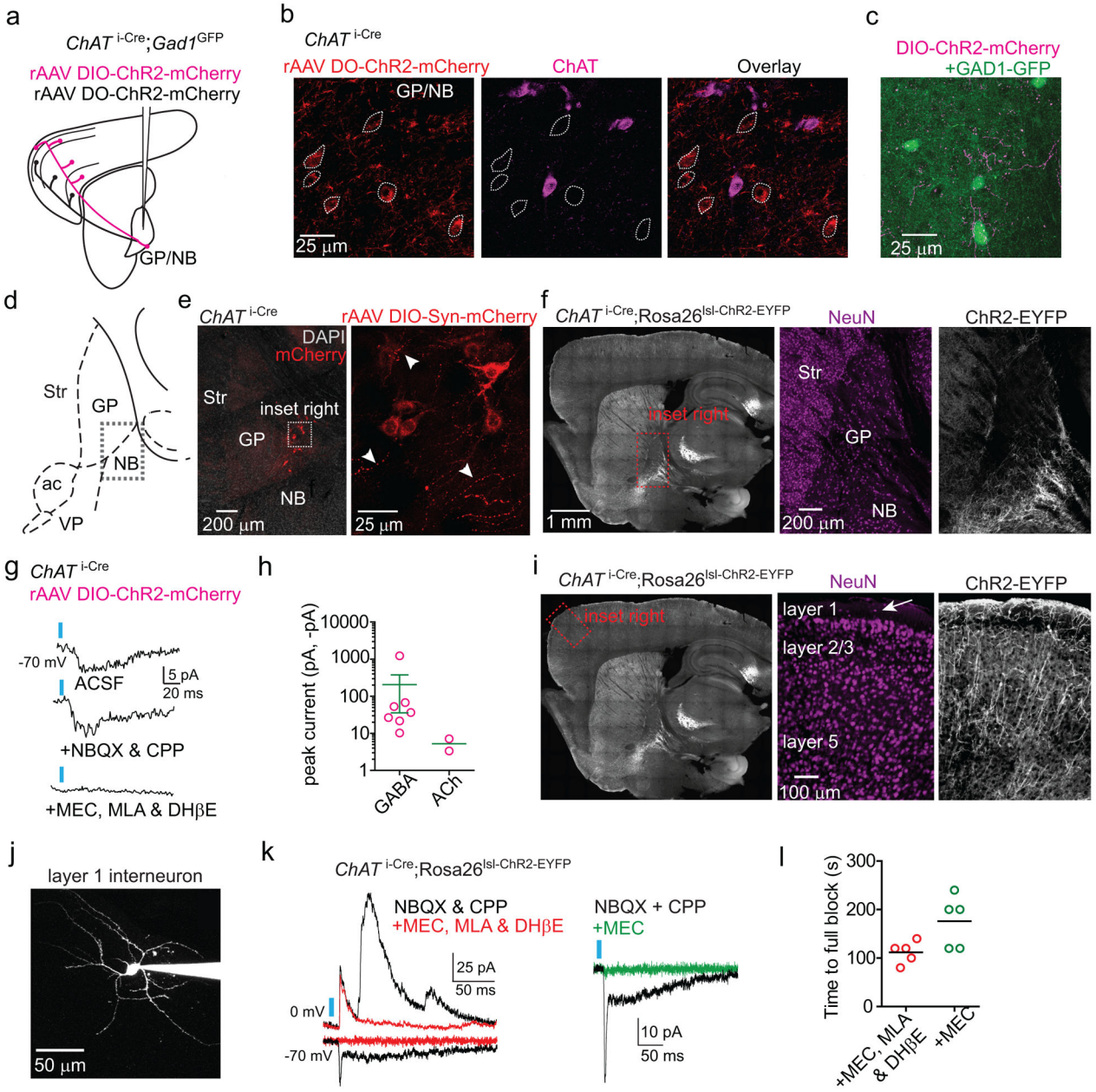

Extended Data Figure 7. ChR2-mediated stimulation of *ChAT* $^{i\text{-}Cre}$ axons following rAAV transduction or with a Cre-activated allele evokes ACh and GABA mediated currents

a,b. Targeting ChR2 expression to ChAT+ and ChAT− GP-FC cells. **a.** Schematic of ChAT + (magenta) or ChAT− (black) GP-FC axons expressing ChR2-mCherry after DIO (Cre-On) or DO (Cre-Off) rAAV transduction in the GP of *ChAT* $^{i\text{-}Cre}$;*GAD1* ^{GFP} mice. **b.** rAAV DO-ChR2-mCherry transduced into the *ChAT* $^{i\text{-}Cre}$ GP expresses ChR2-mCherry selectively in Cre^{-} neurons. Single confocal plane showing neighboring ChR2-mCherry^{+} soma (dotted outline) and ChAT^{+} soma at the GP/NB border. Of n=158 ChR2-mCherry^{+} neurons surrounding n=223 ChAT^{+} neurons, n=0 were ChR2-mCherry^{+}ChAT^{+} (from 2 mice). **c.** ChAT+ axons surrounding *GAD1* ^{GFP} expressing cells in FC layer 6. **d–f**. ChAT+ GP-FC

cells ramify local axon collaterals around the GP/NB border. **d.** Sagittal atlas with the GP/NB border indicated with a dashed box. **e.** *Left*, low magnification view of *ChAT* $^{i\text{-}Cre}$ GP following transduction with rAAV DIO-Synaptophysin-mCherry. DAPI (grey), nuclear stain. *Right*, max projection confocal stack (28 μm) of inset region. Example putative presynaptic boutons indicated by arrowheads. **f.** *Left*, low magnification sagittal section from *ChAT* $^{i\text{-}Cre}$;Rosa26$^{lsl\text{-}ChR2\text{-}EYFP/+}$ mouse. *Right*, high magnification inset of GP showing distribution of neurons (NeuN immunostain, magenta) and ChR2-EYFP^{+} processes (white). **g,h.** Following rAAV transduction in *ChAT* $^{i\text{-}Cre}$ mice, ChR2 activation of local *ChAT* $^{i\text{-}Cre}$ axon collaterals results in rare nicotinic EPSCs but prevalent GABAergic IPSCs onto ChR2^{-} GP/NB neurons (EPSC=2 of 85 cells; IPSC=7 of 85 cells from 6 mice). **g.** Light-evoked EPSC from an example ChR2^{-} GP/NB cell voltage-clamped at −70 mV (*top*) was insensitive to glutamate receptor block with NBQX and CPP (*middle*), but abolished by bath application of MEC, MLA & DHβE (*bottom*), suggesting the EPSC resulted from ACh release and nicotinic receptor activation. **h.** Summary of peaks from nicotinic EPSCs and GABAergic IPSCs evoked from *ChAT* $^{i\text{-}Cre}$ axons onto ChR2^{-} GP/NB cells. **i.** *Left*, low magnification image of sagittal section from a *ChAT* $^{i\text{-}Cre}$;Rosa26$^{lsl\text{-}ChR2\text{-}EYFP/+}$ mouse. *Right*, high magnification of inset from frontal cortex showing distribution of neurons (NeuN immunostain, magenta) and ChR2-EYFP (white), expressed in axons from basal forebrain and in local cortical interneurons. **j.** Maximum intensity 2-photon projection of a layer 1 interneuron following whole-cell recording. **k.** *Left*, light-evoked current responses from two layer 1 interneurons held at indicated potentials to optogenetic activation in a *ChAT* $^{i\text{-}Cre}$;Rosa26$^{lsl\text{-}ChR2\text{-}EYFP/+}$ mouse in baseline conditions (black, NBQX & CPP) and after bath application of nicotinic receptor antagonist cocktail (red, MEC, MLA & DHβE). *Right*, nicotinic EPSCs are blocked by bath application of the non-selective blocker MEC alone (green). **l.** Time until full block of light-evoked nicotinic EPSCs following bath application of either nicotinic receptor antagonist cocktail (MEC, MLA & DhβE, n=5 cells from 3 mice) or MEC alone (n=5 cells from 3 mice). Inter-stimulus interval = 20 s.

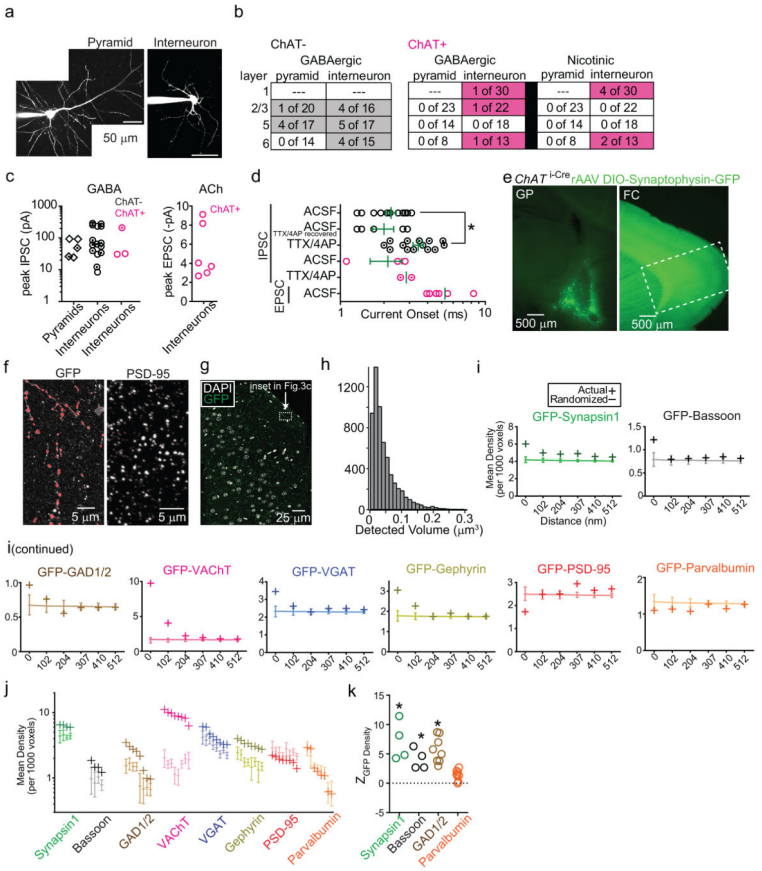

Extended Data Figure 8. Synaptic connectivity and array tomography marker co-localization analysis of GP-FC axons in FC

a–d. Ionotropic synaptic connectivity of ChAT+ and ChAT− GP-FC neurons onto FC cell types and layers. **a.** Example morphologies of FC neurons identified as pyramidal (from layer 5) or an interneuron (from layer 1). **b.** Summary of cortical neurons with ChR2-evoked monosynaptic ionotropic GABAergic or nicotinic currents from ChAT+ or ChAT− axons by cortical layer. **c.** Peak currents induced by ChR2 activation of ChAT+ or ChAT− GP-FC cells in FC. Post-synaptic cells are grouped across layers as pyramids or interneurons. *Left*, GABAergic IPSCs reported with either TTX/4AP in the bath or following wash in are plotted with dotted data. IPSCs recorded in baseline conditions (ChAT−, NBQX & CPP; ChAT+, ACSF only) and are plotted with undotted data. Each cell is represented once. (ChAT−, n=5 pyramids, n=15 interneurons from 13 mice; ChAT+, n=3 interneurons, from 15 mice). *Right*, nicotinic EPSCs recorded in ACSF, present after bath application of CPP and NBQX and fully blocked by nicotinic receptor antagonists (MEC, MLA, DHβE, n=5 interneurons from 15 mice). **d.** Onset latencies for IPSCs and EPSCs induced by ChR2 activation of ChAT+ or ChAT− GP-FC cells under baseline conditions only (“ACSF”) or in the presence of TTX/4AP (“TTX/4AP”). “$\text{Baseline}_{\text{TTX/4AP}}$” refers to the subset of cells with IPSCs recorded under both baseline conditions and recovered following wash in of TTX/4AP (n=5; same data as Fig. 3b). Onset latencies of ChAT− IPSCs were longer in TTX/4AP (n=14) than ACSF (n=11). Asterisk, $P<0.05$ (Mann-Whitney). Bars denote mean ±s.e.m. **e–k.** Array tomography based co-localization analysis of ChAT+ pre-synaptic

terminals (PSTs) in FC. **e.** *Left*, 300 μm sagittal slab from a *ChAT* $^{i\text{-}Cre}$ mouse injected with 300 nl of rAAV DIO-Synaptophysin-GFP in GP. *Right*, box indicates area of FC prepared for array tomography. **f**. Automated detection of GFP^+ volumes ("pearls") and synaptic markers. *Left*, maximum projection of GFP^+ axons following computational detection of string-associated "pearls" (in red). *Right*, a single 70 nm plane showing diffraction-limited immunohistochemical punctae for PSD-95 and computational detection of point sources (in red). **g.** Maximum projection (z=2.17 μm) through layers 1–3 of FC following injection of rAAV DIO-Synaptophysin-GFP into the GP of a *ChAT* $^{i\text{-}Cre}$ mouse. Inset shows location of axon shown in Fig. 3c. h–k. GFP^+ pearls are putative GABAergic PSTs. **h**. Individual volumes for all detected GFP^+ PSTs (n=6,071 pearls from 2 mice; n=4 layers 1 & 2/3 stacks, n=4 layer 5 stacks). **i.** Mean density by distance plots for GFP^+ PSTs versus synapsin1, bassoon, GAD1/2, VAChT, VGAT, Gephyrin, PSD-95 and parvalbumin from example stack. Crosses indicate means from real data, while lines denote mean values following 1000 rounds of marker randomization. Error bars denote 99% confidence intervals. **j.** Mean densities within GFP^+ PSTs (0 distance) for all markers and all stacks. Real and randomized data are indicated as in **i. k.** Z score summary (n=8 stacks) quantifying the differences in mean density for the synaptic markers shown in **j** (and not reported in Fig. 3e) within GFP^+ PSTs (0 distance) for the real data and following 10 rounds of randomization of GFP^+ volumes. Positive Z scores indicate higher densities in the real data. Asterisk, P<0.001 for all stacks.

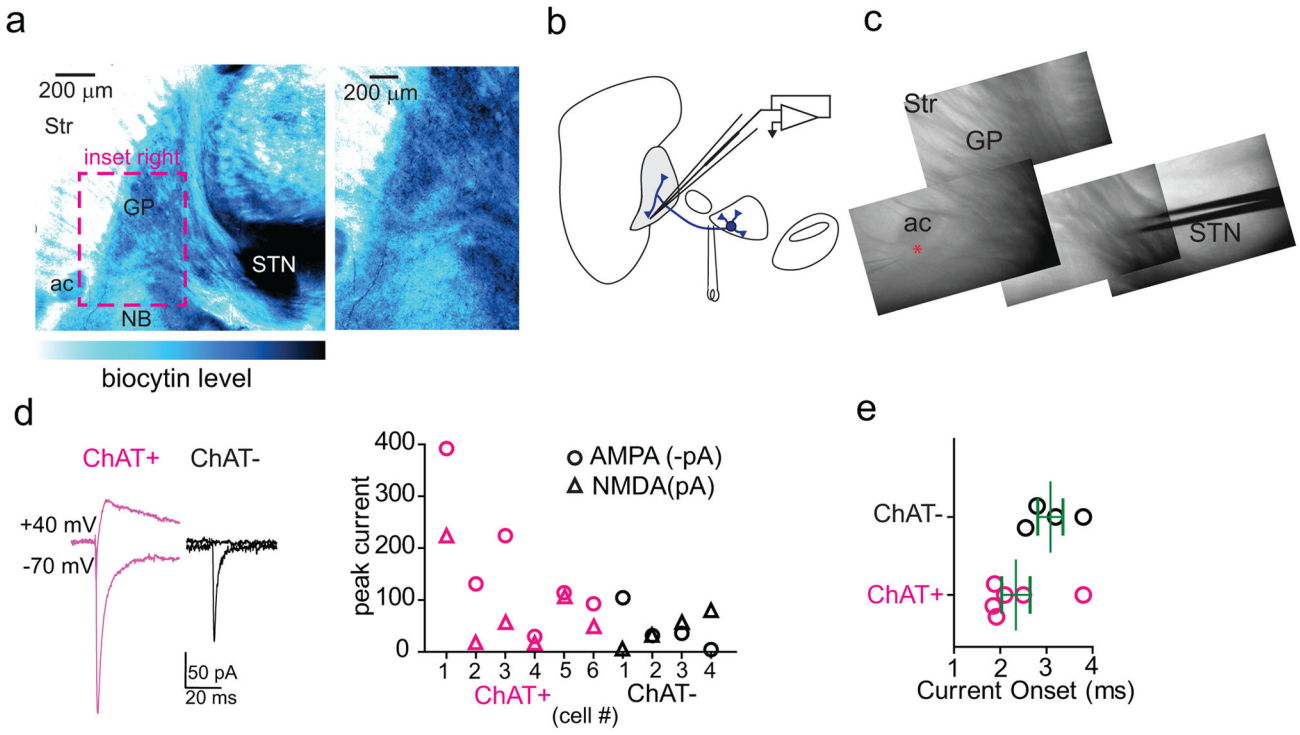

Extended Data Figure 9. GP-FC cells receive glutamatergic synapses from the STN

a. *Left*, low magnification view of parasagittal slice showing the GP following biocytin labeling of the STN and avidin-HRP/DAB visualization of STN projections. *Right*, high

magnification view of inset showing DAB-labeled projections in the GP and around the GP/NB border. **b.** Schematic of experimental strategy to electrically stimulate STN projections to GP. A bipolar electrode was placed at the anterior border of STN and GP-FC cells were targeted for whole-cell voltage-clamp recording. **c.** Acute parasagittal slice showing location of the bipolar electrode and recording pipette (red asterisk). **d,e.** Electrically-evoked glutamatergic currents in GP-FC cells following stimulation of STN-GP axon tract. **d.** *Left*, example NBQX-sensitive AMPAR (V_{hold} = −70 mV) then CPP-sensitive NMDAR (V_{hold} = +40 mV) currents evoked in GP-FC cells under baseline conditions (SR95331, scopolamine, CGP55845). *Right*, summary of AMPAR and NMDAR peak currents in ChAT+ (n=6) and ChAT− (n=4) GP-FC cells (from 7 mice). **e.** Onset latencies of glutamatergic currents (ChAT+: 2.3±0.3 ms, n=6 cells; ChAT−: 3.08±0.3 ms, n=4 cells, from 7 mice). Bars denote mean±s.e.m.

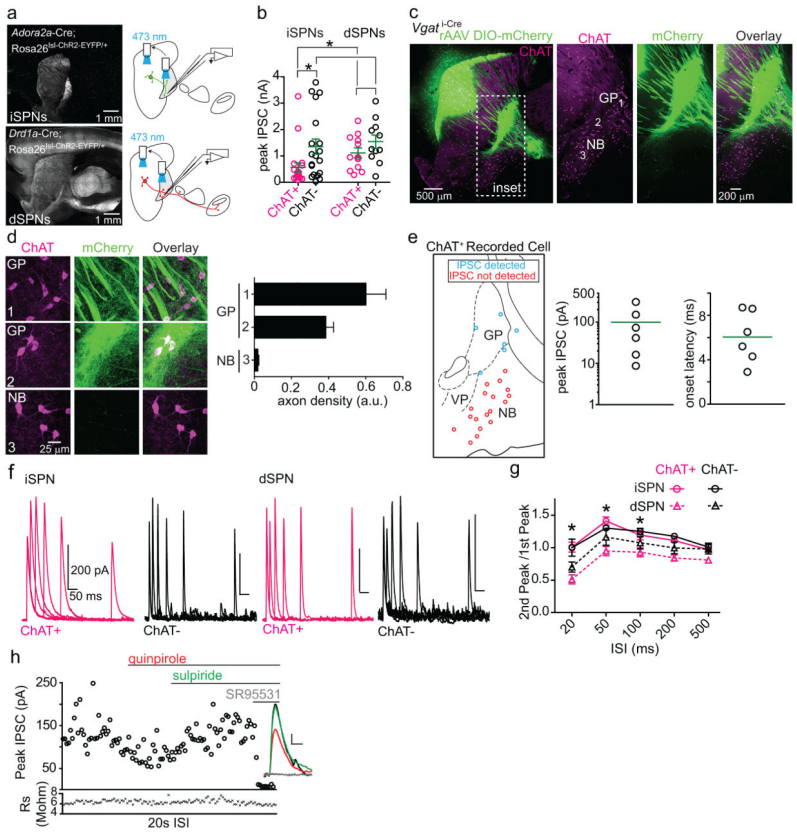

Extended Data Figure 10. GP-FC cells receive GABAergic synapses from dorsal striatal iSPNs and dSPNs with different presynaptic properties and responses to D2r signaling

a. *Left*, sagittal sections from an *Adora2a*-Cre;Rosa26$^{lsl\text{-}ChR2\text{-}EYFP/+}$ (*top*) or *Drd1a*-Cre; Rosa26$^{lsl\text{-}ChR2\text{-}EYFP/+}$ (*bottom*) mouse where ChR2-EYFP is expressed in either iSPNs or dSPNs, respectively. *Middle*, light was delivered first over the recorded cell (peak IPSCs in **b**) and then in dorsal striatum (pharmacological analysis in Fig. 4c;ED Fig. 10h and pre-synaptic properties in **f,g**). **c,d.** SPNs from dorsal striatum arborize axons in and around the GP/NB border but not in the basal forebrain. **c.** *Left*, sagittal section from a *VGAT* $^{i\text{-}Cre}$ mouse injected with rAAV DIO-mCherry into dorsal striatum. *Right*, higher magnification

view of inset. Axons from SPNs arborize in the GP proper and GP/NB border regions (areas 1 and 2) but not in the more ventral region of the basal forebrain (area 3, NB proper/substantia innominata). **d.** *Left*, example maximum projection confocal stacks (z = 28–42 μm) from the inset regions in **c**. *Right*, binary axonal quantification from the regions indicated. SPN axon density is sharply reduced in NB proper/substantia innominata. **e.** Synaptic connectivity screen for dorsal striatal SPN IPSCs onto $ChAT^{+}$ neurons of the GP and basal forebrain. ChAT-GFP mice were injected with Cre-Off rAAV DO-ChR2-mCherry in dorsal striatum and whole-cell recordings were targeted to $ChAT^{+}$ neurons (n=23 cells, from 4 mice) in combination with optogenetic activation. NBQX and CPP were included in the bath to block glutamatergic transmission. *Left*, sagittal map of recording locations of ChAT-GFP^{+} neurons with detected IPSCs (blue) and no detected IPSCs (red). *Right*, peaks and onset latencies for detected IPSCs. Green lines denote means. In every experiment, IPSCs onto ChAT-GFP^{+} neurons of the GP were detected before recordings were targeted to more ventral areas. **f,g.** Paired pulse optogenetic activation of iSPNs (*Adora2a*-Cre;$Rosa26^{lsl\text{-}ChR2\text{-}EYFP/+}$) and dSPNs (*Drd1a*-Cre;$Rosa26^{lsl\text{-}ChR2\text{-}EYFP/+}$) in dorsal striatum reveals differences in short-term synaptic plasticity properties in GP-FC cells. **f.** Examples of optogenetically evoked paired pulse IPSCs (interstimulus interval = 20, 50, 100, 200, and 500 ms) from iSPNs (*left*) and dSPNs (*right*) in GP-FC cells. **g.** Mean $2^{nd}/1^{st}$ peak IPSC ratios (iSPN: n= 13 ChAT+, n=9 ChAT− cells from 11 mice; dSPN: n=9 ChAT+, n=8 ChAT− cells from 6 mice). Asterisk, $P<0.05$ iSPNs vs dSPNs (ChAT+ and ChAT− grouped together, Mann-Whitney); Error bars denote s.e.m. **h.** Example iSPN peak IPSCs in a ChAT − GP-FC cell following application of quinpirole, sulpiride and SR95331. *Inset*, average IPSCs. Scale bar, 20 pA/10 ms. Rs, series resistance.

Supplementary Material

Refer to Web version on PubMed Central for supplementary material.

Acknowledgments

The authors thank the Lowell laboratory at Beth Israel Deaconess Medical Center for the gift of the DIO-Synaptophysin-mCherry and DIO-Synaptophysin-GFP rAAVs, Rachel Pemberton for technical support, Dr. Fenna Krienen, Nicole Duggan, Dr. Pascal Kaeser and members of the Sabatini laboratory for helpful discussions. This work was supported by grants from the National Institute of Health (F31 NS074842) to A.S., (F31-MH093026-01A1) to I.A.O., (P30 EY12196) to the Vision Core and NINDS P30 Core Center grant (#NS072030) to the Neural Imaging Center and Neurobiology Imaging Center in the Department of Neurobiology at Harvard Medical School and an (R01 NS046579) to B.L.S.

References

1. Yin HH, Knowlton BJ. The role of the basal ganglia in habit formation. Nat Rev Neurosci. 2006; 7:464–476. [PubMed: 16715055]
2. Smith Y, Bevan MD, Shink E, Bolam JP. Microcircuitry of the direct and indirect pathways of the basal ganglia. Neuroscience. 1998; 86:353–387. [PubMed: 9881853]
3. Kravitz AV, et al. Regulation of parkinsonian motor behaviours by optogenetic control of basal ganglia circuitry. Nature. 2010; 466:622–626. [PubMed: 20613723]
4. Freeze BS, Kravitz AV, Hammack N, Berke JD, Kreitzer AC. Control of Basal Ganglia Output by Direct and Indirect Pathway Projection Neurons. J Neurosci. 2013; 33:18531–18539. [PubMed: 24259575]

5. Goldberg JH, Farries MA, Fee MS. Basal ganglia output to the thalamus: still a paradox. Trends Neurosci. 2013; 36:695–705. [PubMed: 24188636]
6. Seeman P. Dopamine receptors and the dopamine hypothesis of schizophrenia. Synapse. 2004; 1:133–152. [PubMed: 2905529]
7. Tohen M, Vieta E. Antipsychotic agents in the treatment of bipolar mania. Bipolar Disord. 2009; 11:45–54. [PubMed: 19538685]
8. Bloch MH, et al. A systematic review: antipsychotic augmentation with treatment refractory obsessive-compulsive disorder. Mol Psychiatry. 2006; 11:622–632. [PubMed: 16585942]
9. Kita H. Globus pallidus external segment. Prog Brain Res. 2007; 160:111–133. [PubMed: 17499111]
10. Mesulam MM, Mufson EJ, Levey AI, Wainer BH. Atlas of cholinergic neurons in the forebrain and upper brainstem of the macaque based on monoclonal choline acetyltransferase immunohistochemistry and acetylcholinesterase histochemistry. Neuroscience. 1984; 12:669–686. [PubMed: 6382047]
11. McKinney M, Coyle JT, Hedreen JC. Topographic analysis of the innervation of the rat neocortex and hippocampus by the basal forebrain cholinergic system. J Comp Neurol. 1983; 217:103–121. [PubMed: 6875049]
12. Grove EA, Domesick VB, Nauta WJ. Light microscopic evidence of striatal input to intrapallidal neurons of cholinergic cell group Ch4 in the rat: a study employing the anterograde tracer Phaseolus vulgaris leucoagglutinin (PHA-L). Brain Res. 1986; 367:379–384. [PubMed: 3697714]
13. Henderson Z. The projection from the striatum to the nucleus basalis in the rat: an electron microscopic study. Neuroscience. 1997; 78:943–955. [PubMed: 9174063]
14. Chang HT, Penny GR, Kitai ST. Enkephalinergic-cholinergic interaction in the rat globus pallidus: a pre-embedding double-labeling immunocytochemistry study. Brain Res. 1987; 426:197–203. [PubMed: 3690316]
15. DeLong MR. Activity of pallidal neurons during movement. J Neurophysiol. 1971; 34:414–427. [PubMed: 4997823]
16. Schultz W. Changes in behavior-related neuronal activity in the striatum during learning. Trends Neurosci. 2003; 26:321–328. [PubMed: 12798602]
17. Laplane D, et al. Obsessive-compulsive and other behavioural changes with bilateral basal ganglia lesions. A neuropsychological, magnetic resonance imaging and positron tomography study. Brain. 1989; 112(Pt 3):699–725. [PubMed: 2786440]
18. Tkatch T, Baranauskas G, Surmeier DJ. Basal forebrain neurons adjacent to the globus pallidus co-express GABAergic and cholinergic marker mRNAs. Neuroreport. 1998; 9:1935–1939. [PubMed: 9674570]
19. Mallet N, et al. Dichotomous Organization of the External Globus Pallidus. Neuron. 2012; 74:1075–1086. [PubMed: 22726837]
20. Sarter M, Bruno JP. The neglected constituent of the basal forebrain corticopetal projection system: GABAergic projections. Eur J Neurosci. 2002; 15:1867–1873. [PubMed: 12099892]
21. Saunders A, Johnson CA, Sabatini BL. Novel recombinant adeno-associated viruses for Cre activated and inactivated transgene expression in neurons. Front Neural Circuits. 2012; 6:47. [PubMed: 22866029]
22. Shepherd GM, Harris KM. Three-dimensional structure and composition of CA3-->CA1 axons in rat hippocampal slices: implications for presynaptic connectivity and compartmentalization. J Neurosci. 1998; 18:8300–8310. [PubMed: 9763474]
23. Nambu A, Tokuno H, Takada M. Functional significance of the cortico-subthalamo-pallidal 'hyperdirect' pathway. Neurosci Res. 2002; 43:111–117. [PubMed: 12067746]
24. Albin RL, Young AB, Penney JB. The functional anatomy of basal ganglia disorders. Trends Neurosci. 1989; 12:366–375. [PubMed: 2479133]
25. Simpson EH, Kellendonk C, Kandel E. A Possible Role for the Striatum in the Pathogenesis of the Cognitive Symptoms of Schizophrenia. Neuron. 2010; 65:585–596. [PubMed: 20223196]
26. Ripke S, et al. Biological insights from 108 schizophrenia-associated genetic loci. Nature. 2014; 511:421–427. [PubMed: 25056061]

27. Insel TR. Rethinking schizophrenia. Nature. 2010; 468:187–193. [PubMed: 21068826]
28. Blum BP, Mann JJ. The GABAergic system in schizophrenia. Int J Neuropsychopharma. 2002; 5:159–179.
29. Scarr E, Gibbons AS, Neo J, Udawela M, Dean B. Cholinergic connectivity: it's implications for psychiatric disorders. Front Cell Neurosci. 2013; 7:55. [PubMed: 23653591]
30. Lewis DA, Hashimoto T, Volk DW. Cortical inhibitory neurons and schizophrenia. Nat Rev Neurosci. 2005; 6:312–324. [PubMed: 15803162]
31. Rossi J, et al. Melanocortin-4 Receptors Expressed by Cholinergic Neurons Regulate Energy Balance and Glucose Homeostasis. Cell Metab. 2011; 13:195–204. [PubMed: 21284986]
32. Vong L, et al. Leptin Action on GABAergic Neurons Prevents Obesity and Reduces Inhibitory Tone to POMC Neurons. Neuron. 2011; 71:142–154. [PubMed: 21745644]
33. Taniguchi H, et al. A Resource of Cre Driver Lines for Genetic Targeting of GABAergic Neurons in Cerebral Cortex. Neuron. 2011; 71:995–1013. [PubMed: 21943598]
34. Gong S, et al. Targeting Cre Recombinase to Specific Neuron Populations with Bacterial Artificial Chromosome Constructs. J Neurosci. 2007; 27:9817–9823. [PubMed: 17855595]
35. Gerfen CR, Paletzki R, Heintz N. GENSAT BAC Cre-recombinase driver lines to study the functional organization of cerebral cortical and basal ganglia circuits. Neuron. 2013; 80:1368–1383. [PubMed: 24360541]
36. Tallini YN, et al. BAC transgenic mice express enhanced green fluorescent protein in central and peripheral cholinergic neurons. Phys Genomics. 2006; 27:391–397.
37. Madisen L, et al. A robust and high-throughput Cre reporting and characterization system for the whole mouse brain. Nat Neuro. 2010; 13:133–140.
38. Madisen L, et al. A toolbox of Cre-dependent optogenetic transgenic mice for light-induced activation and silencing. Nat Neuro. 2012:1–12.
39. Tamamaki N, et al. Green fluorescent protein expression and colocalization with calretinin, parvalbumin, and somatostatin in the GAD67-GFP knock-in mouse. J Comp Neurol. 2003; 467:60–79. [PubMed: 14574680]
40. Saunders A, Johnson CA, Sabatini BL. Novel recombinant adeno-associated viruses for Cre activated and inactivated transgene expression in neurons. Front Neural Circuits. 2012; 6:47. [PubMed: 22866029]
41. Mesulam MM, Mufson EJ, Levey AI, Wainer BH. Cholinergic innervation of cortex by the basal forebrain: cytochemistry and cortical connections of the septal area, diagonal band nuclei, nucleus basalis (substantia innominata), and hypothalamus in the rhesus monkey. J Comp Neurol. 1983; 214:170–197. [PubMed: 6841683]
42. Beurrier C, Ben-Ari Y, Hammond C. Preservation of the direct and indirect pathways in an in vitro preparation of the mouse basal ganglia. Neuroscience. 2006; 140:77–86. [PubMed: 16580149]
43. Marx M, Günter RH, Hucko W, Radnikow G, Feldmeyer D. Improved biocytin labeling and neuronal 3D reconstruction. Nat Protoc. 2012; 7:394–407. [PubMed: 22301777]
44. Freeze BS, Kravitz AV, Hammack N, Berke JD, Kreitzer AC. Control of Basal Ganglia Output by Direct and Indirect Pathway Projection Neurons. J Neurosci. 2013; 33:18531–18539. [PubMed: 24259575]
45. Eberly D, Gardner R, Morse B, Pizer S, Scharlach C. Ridges for image analysis. Journal of Mathematical Imaging and Vision. 1994; 4:353–373.
46. Canny J. A computational approach to edge detection. IEEE Trans Pattern Anal Mach Intell. 1986; 8:679–698. [PubMed: 21869365]

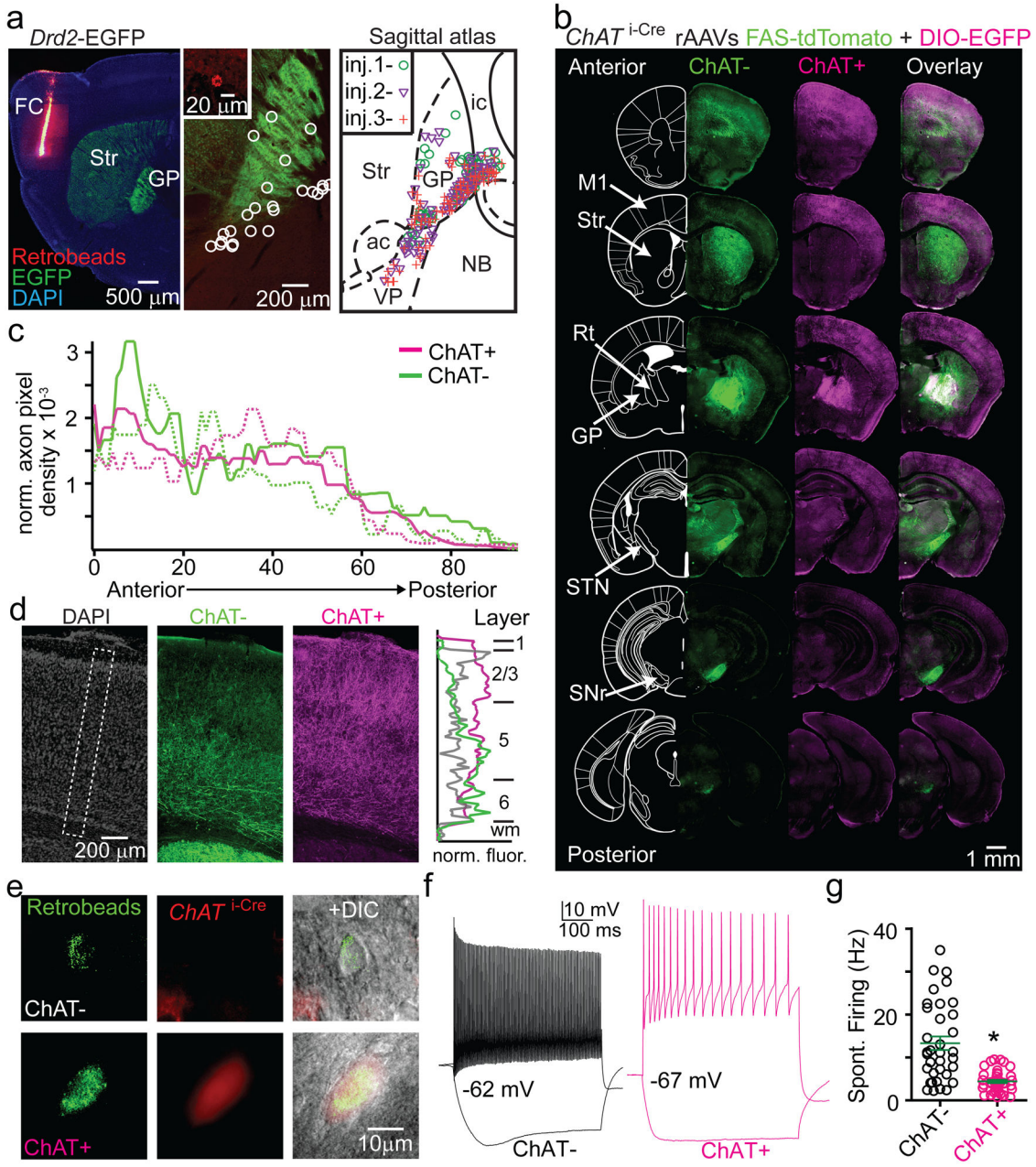

Figure 1. The GP and bordering NB contain two cell types that project to FC

a. *Left*, sagittal section from a *Drd2*-EGFP mouse injected with retrobeads into FC. *Center*, retrobead^{+} neurons (inset and circle-highlighted) in a medial section of GP. *Right*, retrobead^{+} overlay from 3 separate injections, spanning ~300 µm and excluding ventral basal forebrain. ac, anterior commissure; ic, internal capsule; Str, striatum; VP, ventral pallidum. **b–d.** Anterograde labeling of ChAT+ and ChAT− GP-FC axons. **b.** Coronal sections from a *ChAT* $^{i\text{-}Cre}$ mouse injected in GP (EDFig. 3g) with rAAVs DIO-EGFP (Cre-On) and FAS-tdTomato (Cre-Off) sampled from a whole-brain reconstruction. M1, primary motor cortex; Rt, thalamic reticular nucleus; STN, subthalamic nucleus; SNr, substantia nigra reticulata. **c.** Anterior-posterior distribution of normalized ChAT+ and ChAT− cortical

axon densities (2 mice, solid and dotted lines). **d.** *Left,* GP-FC axons across layers in anterior M1. *Right,* normalized average fluorescence from dotted box. **e.** ChAT+ and ChAT− GP-FC cells are distinguishable in acute brain slices following green retrobead injection in FC of *ChAT* $^{i\text{-}Cre}$;Rosa26$^{lsl\text{-}tdTomato}$ mice. **f.** Example membrane voltage (V_m) traces for GP-FC cells following positive (ChAT+:1.7; ChAT−:0.9 nA) and negative (ChAT+:−0.2; ChAT−: −0.1 nA) current injections (500 ms) to determine maximum firing rates and hyperpolarized membrane properties. Resting V_m is indicated. **g.** Whole-cell spontaneous firing rates (n=45 ChAT+ cells, n=35 ChAT−, 10 mice). Asterisk, P<0.05 (Mann-Whitney).

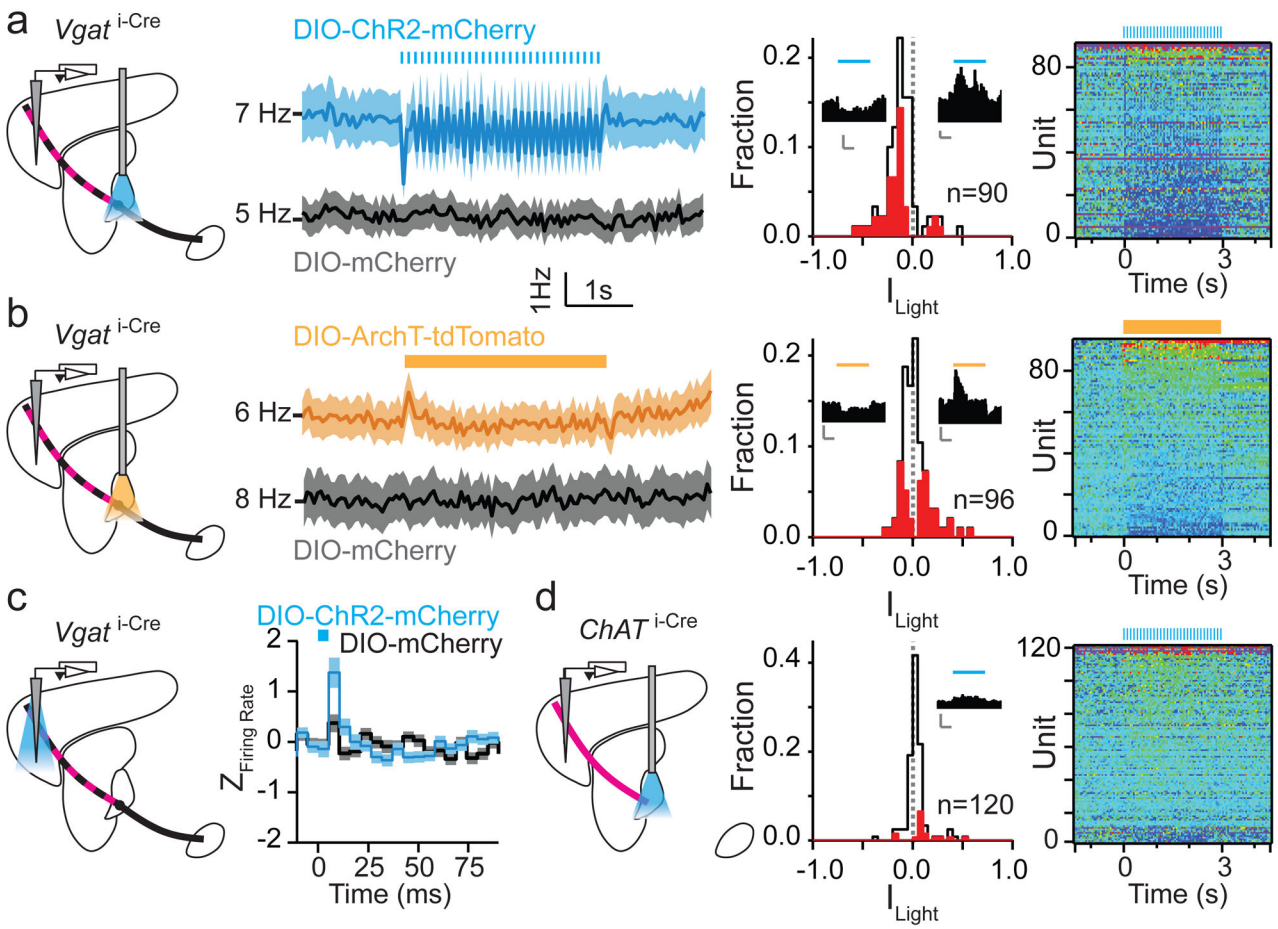

Figure 2. GP-FC cells modulate FC firing rates *in vivo*

a–b. ChR2 stimulation or ArchT inhibition of *Vgat* $^{i\text{-}Cre}$ GP somata bidirectionally modulates firing rates in FC. *Left*, Schematic showing extracellular recordings in FC during optical stimulation of ChAT^{+} (axons shown in magenta) and ChAT^{-} (axons shown in black) in GP with pulsed 473 nm (5ms pulses, 10 Hz for 3s, **a**) or constant 594 nm (3s, **b**) illumination. The mixed ChAT+/ChAT− GP-FC projection appears striped. *Middle left*, mean firing rate (±sem) of all FC units in response to 473 nm stimulation (**a)** of ChR2^{+} (blue; n=90 units, 5 mice) or control (black; n=99 units, 3 mice) mice or 594 nm stimulation (**b**) of ArchT^{+} (yellow; n=96 units, 3 mice) or control mCherry^{+} (black; n=63, 2 mice) mice (*ChAT* $^{i\text{-}Cre}$ mice expressing mCherry in GP). *Middle right*, histogram of indices of light modulation (I_{light}) of FC unit firing rates (f), calculated as ($f_{\text{Light On}} - f_{\text{Light Off}}$)/($f_{\text{Light On}} + f_{\text{Light Off}}$). Red bars indicate significantly modulated units (P<0.05, T-Test). ChR2^{+} stimulation excited 4 and inhibited 38 units; ArchT^{+} stimulation excited 25 and inhibited 19 units. *Insets*, example units, scale bar 5 Hz/1 s. *Right*, pseudocolored plot of changes in f for each unit, normalized to the baseline period and ordered by I_{Light}. **c.** Pulsed (as in **a**) ChR2 stimulation of *Vgat* $^{i\text{-}Cre}$ GP axons in FC increases firing rates on a millisecond time scale. *Left*, Schematic shown optrode placement in FC used for stimulation and recording. *Right*, mean (±sem) Z-scored firing rates after each 5ms light pulse (blue rectangle) relative to equivalent baseline period 3s prior (ChR2^{+}, n=111, 5 mice; mCherry^{+}, n=92, 2 mice). **d.**

Pulsed ChR2 depolarization of *ChAT* $^{i\text{-}Cre}$ GP somata increases firing rates in FC. *Left*, experimental schematic (as in **a**). *Middle*, histogram of I_{light} for FC units (as in **a**), ChR2^{+} excited 15 and inhibited 2 of 120 units from 4 mice. *Right*, pseudocolored plot of changes in firing rate for all units.

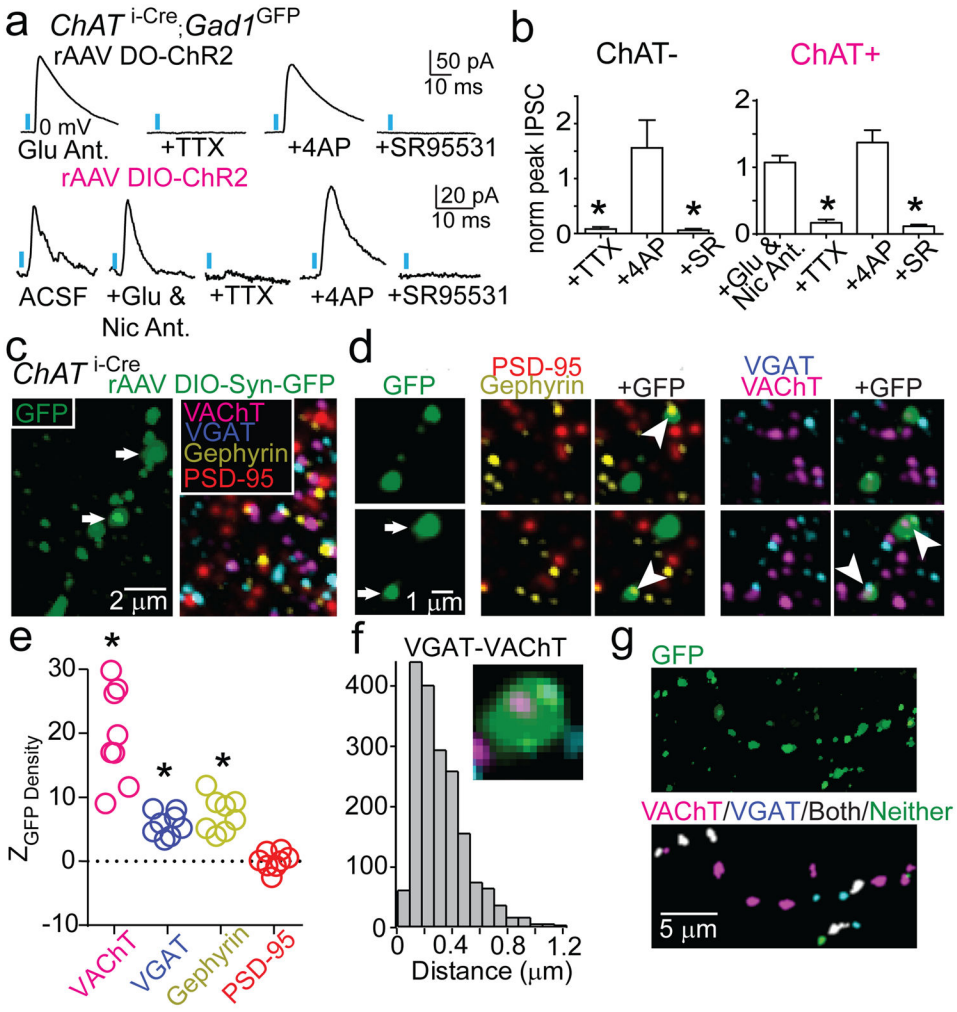

Figure 3. GP-FC cells release GABA and ACh in FC

a–b. DIO (Cre-On) or DO (Cre-Off) rAAV transduction in the GP of *ChAT* $^{i\text{-}Cre}$;*GAD1*^{GFP} mice targets ChR2 to ChAT+ or ChAT− GP neurons.

a. *Top*, IPSCs in a layer 6 interneuron evoked by optogenetic activation of ChAT− axons under baseline conditions of glutamate receptor antagonism (NBQX and CPP) and following co-application of (from *left* to *right*) voltage-gated sodium channel blocker TTX, voltage-gated K^+ channel blocker 4-aminopyridine (4AP) and the $GABA_A$ receptor antagonist SR95531. *Bottom*, IPSCs in a $ChR2^-$ neuron at the GP/NB border following optogenetic activation of surrounding ChAT+ cells under baseline conditions (ACSF) and following co-application of glutamate (NBQX & CPP) and nicotinic (MEC, MLA & DHβE) receptor antagonists, TTX, 4AP and SR95531.

b. IPSC peaks across conditions normalized to baseline (ChAT−, n=5 cortical interneurons; ChAT+, n=7 $ChR2^-$ GP/NB cells). **c–g.** Co-localization analysis of virally labeled ChAT+ pre-synaptic axon terminals (PSTs) in FC using array tomography. **c.** *Left*, maximum projection (z=2.17 μm) through layer 1 of FC showing GFP^+ axon following injection of rAAV DIO-Synaptophysin-GFP into the GP of a *ChAT* $^{i\text{-}Cre}$ mouse. *Right*, a single plane of immunohistochemical labeling. **d.** Consecutive z-planes illustrating synaptic marker

association with GFP$^+$ PSTs (arrows in **c**). PSTs abut Gephyrin but not PSD-95 and contain both VGAT and VAChT punctae (arrowheads). **e.** Z scores for mean marker densities within GFP$^+$ PSTs for real vs. PST-randomized data (n=8 stacks), indicating higher densities in the real data. Asterisk, P<0.001 for all stacks. **f.** Centroid separation of VGAT and VAChT punctae within the same GFP$^+$ PST (n=1,851 comparisons).
g. *Left*, maximum projection of GFP$^+$ axon in layer 1. *Right*, GFP$^+$ PSTs color-coded by VGAT/VAChT identity.

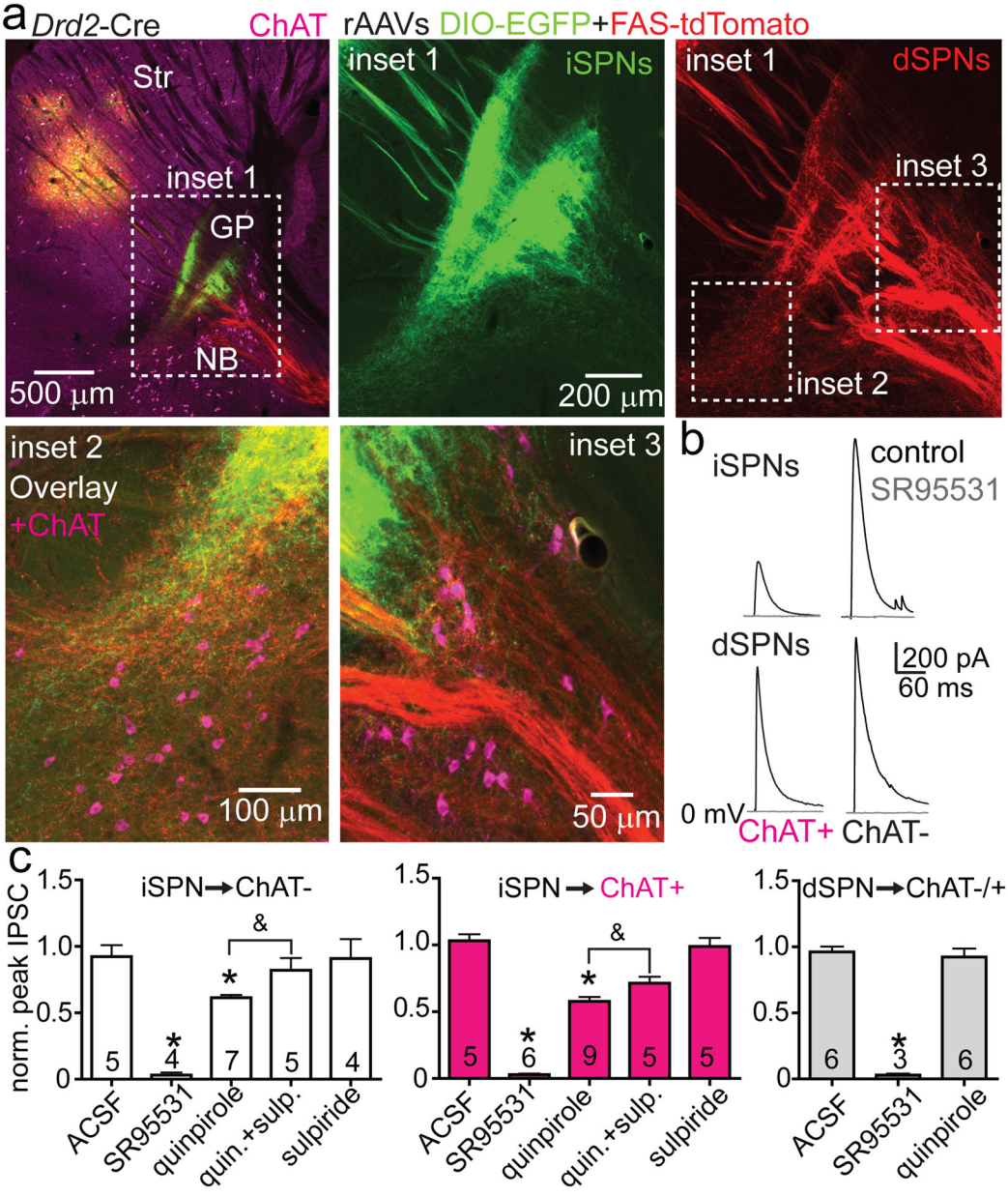

Figure 4. The GP-FC projection is a BG output sensitive to anti-psychotic drugs

a. *Top left*, sagittal section from a *Drd2*-Cre mouse injected with rAAVs DIO-EGFP (Cre-On) and FAS-TdTomato (Cre-Off) into dorsal striatum. *Inset 1*, iSPN and dSPN innervation zones in relation to ChAT+ GP cells. *Insets 2* and *3*, ChAT+ GP-FC clusters. **b.** Optogenetic activation of iSPNs (*Adora2a*-Cre;Rosa26$^{lsl\text{-}ChR2\text{-}EYFP/+}$ mice, *top*) or dSPNs (*Drd1a*-Cre; Rosa26$^{lsl\text{-}ChR2\text{-}EYFP/+}$ mice, *bottom*) in dorsal striatum evoked SR95531-sensitive IPSCs in ChAT+ and ChAT− cells. **c.** iSPN but not dSPN IPSCs are decreased through D2r activation and reversed by an anti-psychotic. Mean IPSCs amplitudes normalized to baseline. Cell numbers are indicated. Asterisk, P<0.05 vs. ACSF (Mann-Whitney); ampersand, P<0.05

quinpirole vs. quinpirole + sulpiride (Paired T-test on cells with both conditions, n=5). Error bars denote s.e.m.